

Nanostructured Coatings for Antimicrobial Applications

Elliot Barron

G20590952

MSc (by Research)

University of Central Lancashire

Project Supervisor – Dr Antonios Kelarakis

October 2017

Contents

Declaration of Work.....	3
Acknowledgements	4
List of Tables	5
List of Figures	5
List of equations	6
Glossary	6
Abstract	7
1. Introduction	8
1.1 Antimicrobial Resistance	8
1.2 Antimicrobial Materials.....	9
1.2.1 Copper	9
1.2.2 Silver Nanoparticles	10
1.2.3 Quaternary Ammonium Salts	11
1.3 Coating Methods	11
1.3.1 Layer-by-layer	11
1.3.2 Dipping.....	12
1.3.3 Spray Assisted.....	13
1.3.4 Spin Coating	13
1.3.5 LbL Equipment	13
1.4 Effect of pH and Salt Concentration on LbL Assemblies	14
1.4.1 Polarity of surface coatings	15
1.4.2 Adsorption Kinetics	15
1.5 Ideal antimicrobial surfaces.....	16
1.6 Applications of surface coatings	17
1.7 Lysozyme	19
1.7.1 Lysozyme Orientation	19
1.7.2 Antimicrobial Properties.....	21
1.8 Nafion.....	24
1.9 Chitosan.....	27
2. Materials and Methodology.....	31
2.1 Materials	31
2.2 Methodology	33
2.2.1 Quartz Crystal Microbalance with Dissipation Monitoring	33

2.2.2 Pre-coating of Gold Crystals	35
2.2.3 Atomic Force Microscopy	36
2.2.4. Contact Angle Measurement	37
2.2.5 Fourier Transform Infrared Spectroscopy (FT-IR).....	37
2.2.6 Scanning Electron Microscope	38
2.2.7 Transparency Test	38
2.2.8 Antimicrobial Activity Testing	38
3. Results and Discussion	40
3.1 Precipitates	40
3.2 SEM	43
3.3 QCM-D.....	45
3.4 AFM.....	53
3.5 Contact Angle Measurements	55
3.6 Antimicrobial Activity.....	58
3.7 Transparency Test	61
4. Summary.....	64
5. Conclusion.....	65
References	66
Supplementary Data	83

Declaration of Work

I declare that while registered as a candidate for the research degree, I have not been a registered candidate or enrolled student for another award of the University or other academic or professional institution. I declare that no material contained in the thesis has been used in any other submission for an academic award and is solely my own work.

Signature of Candidate 

Type of Award MsC (By Research)

School School of Physical Sciences and Computing

Acknowledgements

I would like to express my sincere gratitude to Dr Antonios Kellarakis for his help and expertise in the planning and development of this research. I am grateful for his time and support during the period we have been working together.

I would also like to thank the School of Pharmacy and Biomedical Sciences for their support and assistance throughout, especially Ella Gibbons for her assistance with antibacterial analysis.

List of Tables

Table 1	16
Table 2.....	31
Table 3	32
Table 4.....	55
Table 5	56

List of Figures

Figure 1	8
Figure 2.....	12
Figure 3.....	19
Figure 4.....	20
Figure 5.....	21
Figure 6.....	22
Figure 7.....	22
Figure 8.....	24
Figure 9	24
Figure 10.....	26
Figure 11.....	27
Figure 12	29
Figure 13.....	29
Figure 14.....	34
Figure 15.....	35
Figure 16.....	40
Figure 17.....	40
Figure 18.....	42
Figure 19.....	43
Figure 20.....	44
Figure 21.....	45
Figure 22.....	46
Figure 23.....	46
Figure 24.....	47
Figure 25.....	47
Figure 26.....	48
Figure 27.....	49
Figure 28.....	53
Figure 29.....	58
Figure 30.....	60
Figure 31.....	61

List of equations

Equation 1.....	14
Equation 2.....	16
Equation 3.....	33

Glossary

LbL	Layer by Layer
TBT	Tributyltin
PVC	Poly Vinyl Chloride
MRSA	Methicillin Resistant Staphylococcus Aureus
Ag NPs	Silver Nanoparticles
QAS	Quaternary Ammonium Salts
NMR	Nuclear Magnetic Resonance
MAS	Magic Angle Spinning
QCM-D	Quartz Crystal Microbalance with Dissipation
AFM	Atomic Force Microscopy
FITR	Fourier Transform Infrared Spectroscopy
SEM	Scanning Electron Microscope
S. aureus	Staphylococcus Aureus
E. coli	Escherichia Coli
PSS	Poly(sodium4-styrenesulfonate)
PAH	Poly(allylamine hydrochloride)
PLGA	Poly(D, L-lactide-co-glycolid acid)
pSi	Porous silicon
pDEAEA	Poly(2-diethylaminoethyl acrylate)
NAG	N-acetyl glucosamine
NAM	N-acetyl muramic acid

Abstract

In this study, novel layer by layer assemblies based on Nafion, lysozyme and chitosan were developed and assessed with respect to their antimicrobial activity. A quartz crystal microbalance was used to monitor the built up of the multilayers in real time, confirming the presence of strong electrostatic interactions between the negatively charged Nafion and the positively charged particles of lysozyme and chitosan. The coatings are durable and resist detachment against flowing water, while AFM characterization reveals the presence of a complex surface topology with a high degree of roughness. The wettability of the coated surfaces reflects an interplay between the chemical nature of the deposited materials and the surface morphological characteristics. Moreover, it was observed that the antimicrobial behaviour of the coatings critically depends on the nature and the pH of the deposited layers. The ultrathin coatings comprising 6 bilayers of Nafion/lysozyme (pH=6.2) were shown to exhibit excellent antimicrobial properties, inhibiting the growth of *Staphylococcus aureus* and *Escherichia coli* by a factor of 100%. This remarkable behaviour carries great promise for the development of a new generation of highly effective antimicrobial coatings.

1. Introduction

1.1 Antimicrobial Resistance

Antibiotic resistance is a growing and continuous problem all over the world due to antibiotics being overused for both human and agricultural purposes, which has ultimately led to the major cause for concern in public health. ^[1] One way to address this problem is to reduce the spread of bacteria which can be done is by coating commonly used surfaces with an antimicrobial coating. Antimicrobial coatings can be made via the process of layer by layer (LbL) adhesion which will be discussed in depth during this report.

The purpose of this research project was to surpass previous findings and advance this type of material forward. As stated below on the timeline (Figure 1) there has been research on this topic since 1625 which shows its importance. Metals such as copper and silver are still being used today despite their limitations. Tributyltin (TBT) was previously used but it was banned during 2003-2008 due to it causing damage to the endocrine systems of shell-fish and the immune systems of other organisms. Novel environmentally acceptable alternatives were introduced in 2003 because of TBT and the work done in this project was aimed to continue the exploration of this area ^[2].

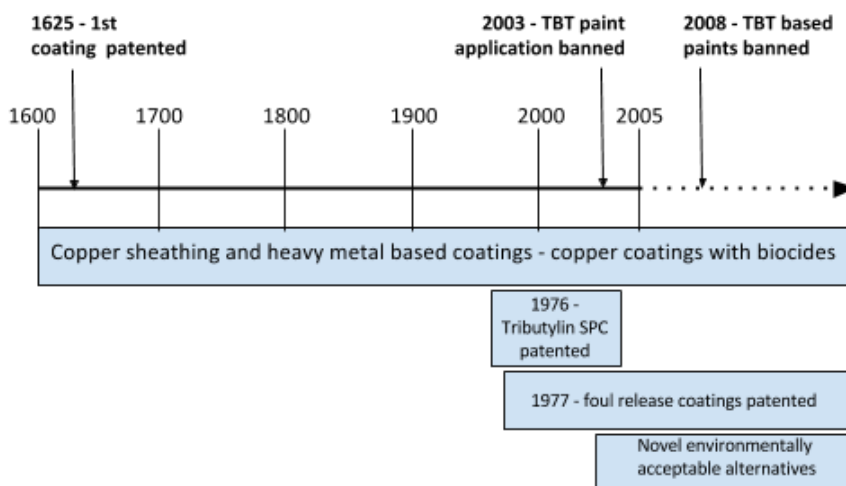


Figure 1. The development on surface coatings over time ^[3]

1.2 Antimicrobial Materials

The development of antimicrobial materials is very important, particularly in the maintenance of hospitals and healthcare environments where hygiene levels need to be maintained to a high standard. Preventative measures such as surface coatings, as well as treatments that inactivate microbes adhered to surfaces, can be used. ^[4]

Poly(vinyl chloride) (PVC). PVC is a versatile, low cost, highly resistant plastic that is used in industry for medical devices, packaging, bottles and boxes. ^[5] Systematic studies aim to improve the antimicrobial resistance of PVC. A study has shown that the use of a biocide agent can be used when bound to the surface or upon release to the surrounding area. The key biocide agents that can be used are copper, silver and quaternary ammonium salts ^[6] and these are detailed below.

1.2.1 Copper

Copper (Cu) is a popular material that is used to reduce infections caused by common microbes such as *Staphylococcus aureus* (*S. aureus*) and *Escherichia coli* (*E. coli*) ^[7]. Cu is commonly used in hospitals, especially on equipment such as bed and door handles, drip-feed equipment and nurse 'help' buttons. Using materials coated with copper reduced the incidence of infection by over 95% and thus contributed to the increased levels of hygiene within the hospitals. ^[8]

The antimicrobial effect of Cu has been tested and documented for a long time with a study by Keevil and Lewis ^[9] showing how Cu can target all parts of the bacteria cell by a series of deactivation mechanisms. It is suggested that the Cu may form free radicals that can deactivate bacteria cells and virus'. The radicals that are formed are highly reactive and deactivation of the protein occurs due to Cu²⁺ ions forming protein chelates with carboxylate and amine groups and by also oxidation of protein and lipids. ^[10]

Cu²⁺ may break the hydrogen bonds of the DNA's double strand leading to the deactivation of microbes. Cu can also disrupt the helical structure of DNA by cross

linking within the strands and it can form bonds with mRNA, which are molecules that play a vital role within DNA. ^[11]

Cu-based spray coating ^[12] is particularly effective in construction working areas where resources like steel are used. The sprays can contain a number of components enhancing a range of the physio-chemical properties of the coated materials ^[8], including the antimicrobial effect. A study by Helfritsch et al ^[13] explains the methods of how the copper can be sprayed onto the surface: the most common are arc, plasma and cold spraying. Although each technique results in a distinctly different microstructure, they all impart significant antimicrobial performance.

With the arc spraying technique, there was a clear relationship between the porosity, the distribution of particle size and antimicrobial activity ^[14].

Different morphologies can also determine how much of an antimicrobial effect there will be, for example Cu surfaces that have high levels of roughness and high surface free energy displayed good antimicrobial activity towards MRSA. ^[15] However, one the major limitations of using Cu is that is that it expensive and has weak mechanical properties when comparing it with stainless steel. ^[16]

1.2.2 Silver Nanoparticles

Silver nanoparticles (Ag NPs) are widely used as antimicrobial agents. Kim *et al* tested Ag using agar plates against *S. aureus*, *E. coli* and yeast which showed a clear inhibition of growth ^[17]. Ag NPs can be deposited by various methods to impart antimicrobial resistance to surfaces. For example, Ag NPs are deposited to fabrics in hygienic clothing by vacuum coating, a method that relies on the ionisation of the sputtering species in the presence of highly-charged pulses ^[18].

Although Ag NPs are highly effective antimicrobial agents, they tend to become concentrated in aquatic environments and are toxic towards organisms that live there. If Ag NPs are used in an increasing number of applications, they might cause significant environmental damage and has adverse effects in humans. ^{[19] [20]} For those reasons, the use of Ag NPs should be strictly regulated and remain beyond certain levels.

1.2.3 Quaternary Ammonium Salts

Quaternary ammonium salts (QAS) are also used as biocides. These salts have low toxicity, low skin irritation, low environmental impact and can penetrate the cell membrane efficiently.^[21] The overall positive charge of the QAS drives the attraction to the overall negative charge of the bacteria's cell membrane.^[22] After this initial attraction, the hydrophobic group on the QAS will cause disruptions in the cytoplasm of the membrane causing the releasing of potassium which leads to cell death.^[23] While QAS are known to be effective antimicrobials, their use is rather limited. This is because they cannot easily be incorporated into a polymer matrix due to poor adhesion and low structural stability.^[24] Antimicrobial activity is mostly dependent on the concentration of biocides on the fibre surface, however reaching such high QAS surface concentrations on plastic materials is challenging.^[25]

All the materials above show good responses to microbes, however they all have significant downfalls. The threat of antibiotic resistance is becoming a global threat and so the most effective methods need to be employed. New medicines that are more capable of fighting multi-resistant bacteria need to be developed, but there also needs to be improvements made to prevent spread of infection in the first place, particularly in public and medical areas. It seems that strong and stable surface coatings that can be applied will help this problem significantly.^[26] The methods by which these coatings can be applied will be explored in the next section.

1.3 Coating Methods

1.3.1 Layer-by-layer

The basic principles of LbL consist of electrostatic interactions between negatively and positively charged materials and other intermolecular forces such as van der Waals and hydrogen bonds. The procedure involves a charged material being submerged in an oppositely charged solution to form the first monolayer. This monolayer is then washed with water to remove excess compounds and the cycle is repeated until multilayers of strongly bonded materials are formed. The morphology, depth and stability of the multilayer film can differ due to the LbL composition.^[27] As the substrates are used in

excess there is no stoichiometric measures of charges used for each step, this allows for a more favourable surface for adhesion of the next layer that is added. [28]

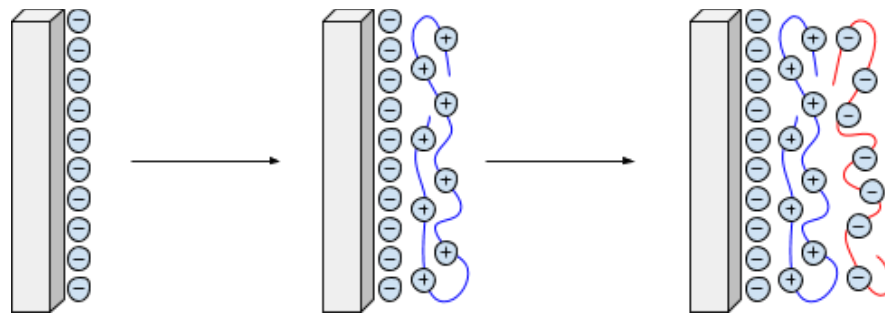


Figure 2. Electrostatic forces of attraction between layers in LbL assemblies [29]

In LbL assemblies, as shown in Figure 2, electrostatic forces of attraction between the building layers give rise to strong and durable coatings. The most common strategies to develop LbL coatings is via dipping or spray-assisted deposition.

1.3.2 Dipping

The dipping method process involves a surface being immersed consecutively into two suspensions containing positively and negatively charged particles, while the surface is washed-off with water after each deposition step. This technique is popular because of its simplicity, but it does have limitations when applied on a large scale. This is due to the time constraints and there may be contaminations upon dipping in various coatings. [30]

As stated, the coated substrate is immersed with a solvent that removes spare polyelectrolytes that are not bound and water can be used for this. This process helps to prevent the cross contamination of solutions. The polyelectrolytes that are strongly bonded to the substrate will remain on the plate and will not be washed off due to their high levels of surface charge density. These bonds are essential for a successful multilayer adhesion and helps to create a durable surface coating. [31]

If a coated substrate with multilayers adsorbed onto it is left to dry after each step, the growth of the next layers added are hindered due to unfavourable arrangements of the molecules on the top layer. If a moist environment is present, the chains become more

flexible and ionisation increases. This makes the films less dense and therefore greater adhesion occurs.^[32]

1.3.3 Spray Assisted

Spray-assisted LbL was introduced to help deal with the shortcomings of the dipping LbL technique. Here surfaces are held up vertically and sprayed uniformly, in a more time-effective manner. The spray assisted method also has many advantages over other methods used, some of which include; reduced cross contamination due to the substrate not being in contact with the stock liquid, the ability to be automated which can run continuously thus reducing the need for human input and it is easy to use when needed for large scale projects.^[33]

1.3.4 Spin Coating

As well as the two most common methods mentioned previously, there are other methods by which an LbL assembly can be achieved. One of these methods is called spin coating and is demonstrated by Bottino *et al*^[34] where they use this method to develop a highly efficient antimicrobial resorbable membrane, to treat bone infections. The strategy relies in the LbL assembly of poly(sodium4-styrenesulfonate) (PSS) and poly(allylamine hydrochloride) (PAH) on the poly(D, L-lactide-co-glycolid acid) (PLGA) surface. As well as this, the authors also entrapped a water-soluble antibiotic within the top layers for extra antimicrobial effects.

Spin coating can consistently produce films of material however for successful spin-coating, the substrate must suit the size of the equipment being used and it must also be planar. Problems arise in this method as uniformity and final thickness is difficult to control and it is not possible to produce the layers from the same solvent making it less environmentally friendly.^[33]

1.3.5 LbL Equipment

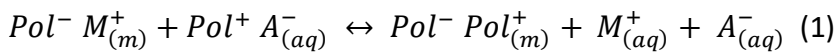
The most commonly used plates for LbL assemblies are made of either silicon, mica, quartz, gold or glass. The texture and morphology of the surface used can affect the levels of adhesion. A treatment of heating and then allowing it to cool with sodium chloride has been to show to smooth out the substrates surface. This creates closer

contact with a larger surface area, which aids the production of a high-quality coat. The elasticity of the coating can also affect the surface adhesion. [35]

The concentrations of the solutions used are the prerequisite for a successful adsorption. This stops the substance from depleting during the LbL process, allows for the concentration to exceed the minimum threshold and reverses the polarity of the charge for each layer. [27]

1.4 Effect of pH and Salt Concentration on LbL Assemblies

A change in the overall pH can lead to the interactions varying between the polymers. This is because changing the pH can have a direct effect on the electrostatic forces between the LbL assemblies and thus immediately affecting the interactions between the substrates and polyelectrolytes. [36]



Equation 1. Shows how a change of pH or concentration of salt dictates the ion exchange regulation of the adsorption step. Where m is molecules that are bonded to the surface of the substrate and aq refers to a molecule that is dissolved (in aqueous state). Pol denotes charged areas of polyelectrolytes and M and A are salt ions.

The equation shows how an increase in the concentration of salt will cause the adsorption step to slow down or stop completely, unless they are removed via dialysis. [37,38] The salt ions between the layers can have an impact on the electrostatic charge. If the threshold of salt concentration is exceeded, there can be a negative impact on adhesion. This is because the overall charge will be decreased as a response to coagulated dispersion. [39] It has been proven that polyelectrolytes can be coated in a media with varying salt concentrations and this results in minimal growth of multilayers beneath thresholds value. [40]

If the pH of the solutions are changed, the separation of polyelectrolytes from the ions will vary the success of adsorption. A change in pH can also affect whether there is a linear or exponential development of multilayers. [41]

1.4.1 Polarity of surface coatings

Studies have been conducted which demonstrate how the polarity of the material can affect the overall LbL system. Aqueous solutions are mainly used for coating materials although non-aqueous materials can be used if they show some form of polarity within the solvent. ^[42] An example of a non-polar solvent is toluene and this can be used by adding surfactants to the suspension of alumina or carbon black. ^[43]

Overall, the materials used for water solution coatings should allow the polyelectrolyte to ionize to a certain extent because the largest interactions present are electrostatic. ^[42]

1.4.2 Adsorption Kinetics

Adsorption kinetics can explain the interaction between a charged colloid and a substrate. The factors that are involved show time-dependence which means their effect can be quantised with adsorption kinetics. There is a two-step process for the adsorption onto the surface of a substrate known as the Johnson Mehl Avrami bi-exponential saturation process. The first step is a first order process that spans over a short amount of time, seconds, where electrostatic anchoring sites on the substrate become unsaturated and this decides if the coating will be successful. The second step stretches over several minutes and reveals how the coated substrates have been rearranged in the first step. ^[44] During this step it is possible that there is more adsorption as a result of the extra polyelectrolyte chains diffusing further. However, the coated substance will eventually become saturated over time. A 'brush like' polyelectrolyte gathering occurs on the surface, which poses as a barrier to further saturation. ^[45]

The Johnson Mehl Avrami process uses an equation that shows the relationship between time, phase fraction transformation and temperature, all based on assumptions. This is shown in equation 2:

$$X(t) = 1 - \exp[-(Kt)^n], K = K_0 \exp\left(-\frac{Q}{RT}\right) \quad (2)$$

Equation 1. The Johnson Mehl Avrami equation (2) where; X (t) represents fraction transformation after time, n shows growth, R shows the gas constant, T shows temperature, Q is the activation energy and K_0 is the coefficient of the pre-exponent. ^[46]

In conclusion, adsorption kinetics should have optimal value to guarantee the best possible conditions for the LbL process and the amount of time the coating solutions are exposed to the substrate should be optimised.

1.5 Ideal antimicrobial surfaces

Bacteria can adhere to almost all natural and synthetic surfaces and another use of antimicrobial coatings could be in operative implants to reduce the risk of infection. Below is a table highlighting the key features of an ideal antimicrobial surface, specific to implant's. These features occur in other applications of surface coatings. ^[47]

Table 1. Ideal antimicrobial surface coating properties ^[47]

Safety	In vitro activity	Efficacy	Easy to use	Market
No systemic toxicity	No cytotoxicity	Proven to be effective	Easy to handle	Acceptable cost
No local toxicity	Proven antibacterial effects	Case studies	Versatile	Good availability
No unwanted long-term side effects	Large spectrum of activity	Randomised trials	Easily storable	Easy to manufacture

1.6 Applications of surface coatings

One use of LbL assembly is to produce a material with high stability that can be used in drugs where a controlled release is required.^[48] Temperature changes are used to influence the permeability of the barrier made by LbL for the introduction of water-soluble drugs. This means the LbL barrier must be strong yet be able to vary its permeability.^[49]

One method that can be used for the controlled release of content within a LbL system is to disassemble it, with another approach being to destroy the assembly. One way in which disassembly can occur is through the use of salts. Sodium chloride has been studied for this purpose and has proven to be useful due to its electrostatic forces.^[50] However, high salt concentrations are needed to initiate the disassembly process, which results in high, often unwanted release of contents.^[51] There is another challenge when using controlled deletion of layers and that is the bond strengths between the layers can be difficult to deplete.^[52] As well as this, there is also a risk that changes in pH can cause unwanted releases.^[53]

It is possible to have slow, controlled disassemblies by using a combination of polyelectrolyte materials that are biodegradable and by also having some which are non-biodegradable.^[54] The same effect can be seen in poly(β -amino) esters that have cleaving properties when the hydrophobicity modifications hit a critical value. After this point, it rapidly destabilises, and releases occur.^[55]

Another application of the coatings is within fouling release systems^[56]. Surfaces that are underwater for long periods of time may be susceptible to growth of organisms such as algae, mussels and barnacles and this can lead to corrosion and frictional resistance, especially on boats. Antifouling coatings that have previously been used contained biocides which were toxic to aquatic life. A fouling release coating does not completely prevent organisms from reaching the surface but they can reduce the adhesion of such things. A remaining challenge in this area is the development of superior and cost-effective fouling release coatings with minimal toxicity.^[57] Surface engineering in the

nanoscale can prevent bio-adhesion by minimising the points of contact for the microorganisms, giving rise to advanced fouling release systems.

LbL can potentially be used in within drug therapies. LbL techniques make it possible to control various parameters such as thickness and mechanical properties. It also allows for drugs to be entrapped within layers which can control how much of the drug is released and when. This is particularly useful as it will help to produce prolonged release drugs, and this is more beneficial for a patient as it requires taking fewer drugs. However, there is room for more research into the involvement of LbL in drug therapies in the future. ^[58]

Another use for using the layer-by-layer technique is to coat foods with edible coatings. One example of this is using gelatin and chitosan to produce a coating for food such as fresh melon and the results shown that the LbL formation inhibited microbial growth for up to 7 days, it was also reported that the LbL formulation preserved the texture of the fruit also. ^[59]

1.7 Lysozyme

A material that can be used in surface coatings is lysozyme. Lysozyme is an enzyme that is found in bodily secretions such as mucus and tears and is abundant in chicken egg whites. Chicken egg white lysozyme is a polypeptide chain consisting of 129 amino acids with an M_r of 14600. The structure of lysozyme is represented in figure 3 as a space filling molecular model. ^[60] The isoelectric point (pI) of lysozyme is near to 11 which means that in the range of pH's from 4-10 it is positively charged. ^[61]

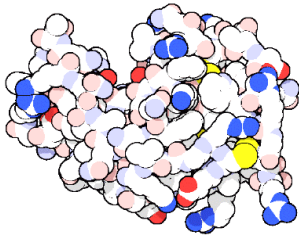


Figure 3. Structure of lysozyme represented by a space filling molecular model ^[62]

From the model (figure 3), it can be seen that the molecule is compact and that most of the polar, hydrophilic side chains are found on the surface of the molecule and can therefore readily interact with the surrounding water. On the inside of the molecule are the hydrophobic, non-polar side chains which therefore means that they are shielded from the solvent as much as possible. Within the molecule there are also two major polypeptide conformations; alpha-helix and the beta-sheets. ^[63]

1.7.1 Lysozyme Orientation

A study has determined that lysozyme molecules have a dimension of 45 x 30 x 30 Å ^[64] which gives them an ellipsoidal shape. Due to their shape, there are two main orientations that are possible; 'side-on' which involves the longer axis of the lysozyme molecule being parallel to the surface and the 'end-on' orientation where the longer axis is at 90° to the surface. However, lysozyme can also adsorb in a way classed as 'edge-on' which is half way between the two previous mentioned orientations (as shown in figure 4). ^[65]

A study by Xu *et al* [66] discusses how lysozyme molecules position themselves in a QCM in LbL assembly, a concept discussed in more detail in section 2.1.2. The study suggests that lysozyme molecules can undergo mild deformation if the surface is too thin, for example less than 1 ng/mm^2 . The most favourable position for lysozymes to position themselves in is side-on and this is how optimum thickness is achieved.

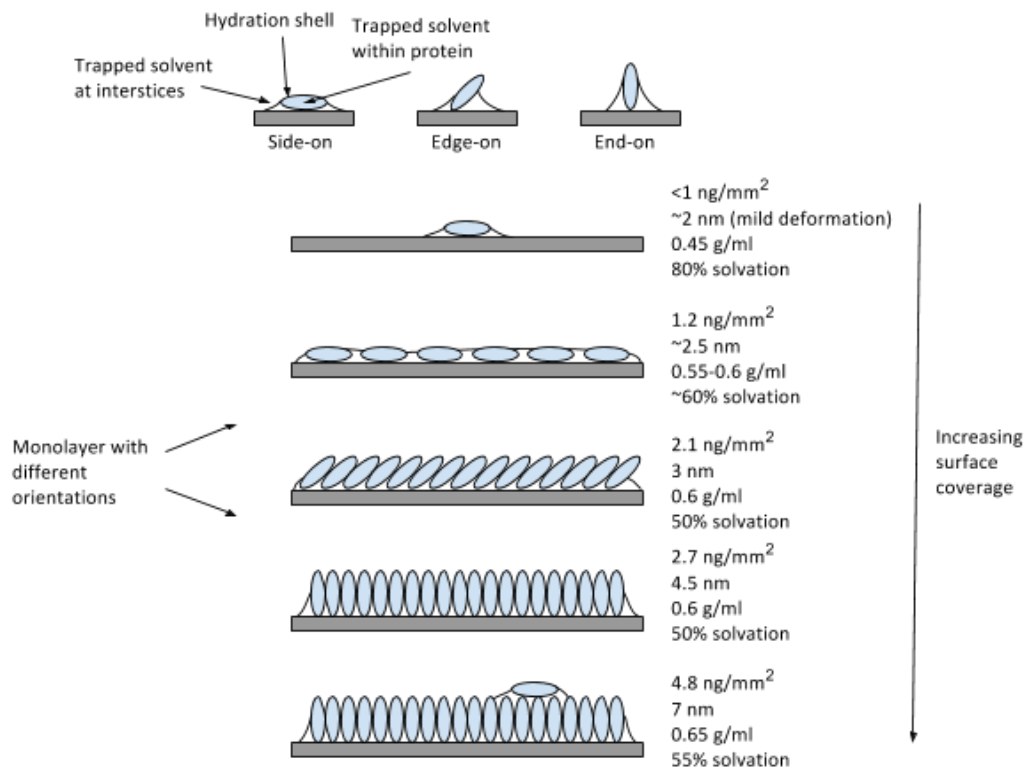


Figure 4. The orientation of lysozyme molecules at different weight percentage solvations. [66]

Lysozyme molecules will adopt different orientations (as shown in figure 4) to increase protein-protein interactions and this can therefore alter the thickness of the layers in a LbL assembly. [67]

Figure 4 also shows that once the thickness increases above 3 nm^2 a multilayer will have been formed. This multilayer will be completely packed with the lysozyme molecules being in the preferred side-on orientation which increases the overall weight percentage solvation. Another way in which the weight percentage solvation can be increased is by rinsing each layer of lysozymes once it has been assembled. The rinsing will remove any loosely-bound lysozymes thus creating gaps through which solvent can penetrate. It has also been shown that the rinsing process can irreversibly reduce the layer thickness as it allows for the lysozymes to stay in the favoured position, side-on (as shown in figure 5). [67]

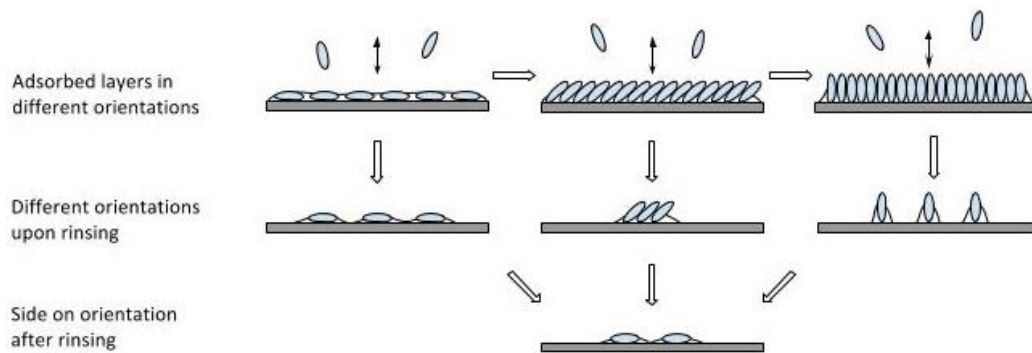


Figure 5. The orientation of lysozyme molecules upon rinsing with water ^[66]

1.7.2 Antimicrobial Properties

The cell walls of bacteria can be destroyed due to lysozyme catalysing the hydrolysis of certain polysaccharides which renders the cell wall vulnerable to osmotic lysis. Lysozymes can bind irreversibly to the transpeptidase enzyme which is essential for when peptidoglycan macromolecules form in synthesis of cell walls, which is similar to the way in which penicillin acts as an antibiotic. ^[68] In standard conditions, bacteria would grow and multiply exponentially in less an hour but when cell wall cross links are damaged, they will be lysed within the media in which they are put. ^[69]

N-acetyl glucosamine (NAG) and N-acetyl muramic acid (NAM) characterise the units which build the structures of bacterial cell walls. Lysozyme is cleaved at (1-4) glycosidic linkages connecting carbon (C1) of NAM to carbon (C4) of NAG. (NAG-NAM)₃ hexasaccharide is the optimum substrate, where lysozyme cleaves at NAM₄--NAG₅ glycosidic bond (shown in figure 6). The active site of lysozyme has six binding sites for each sugar ring of hexacasaccharide. The lysozyme will most likely cleave glycosidic as indicated on figure 6. ^[70]

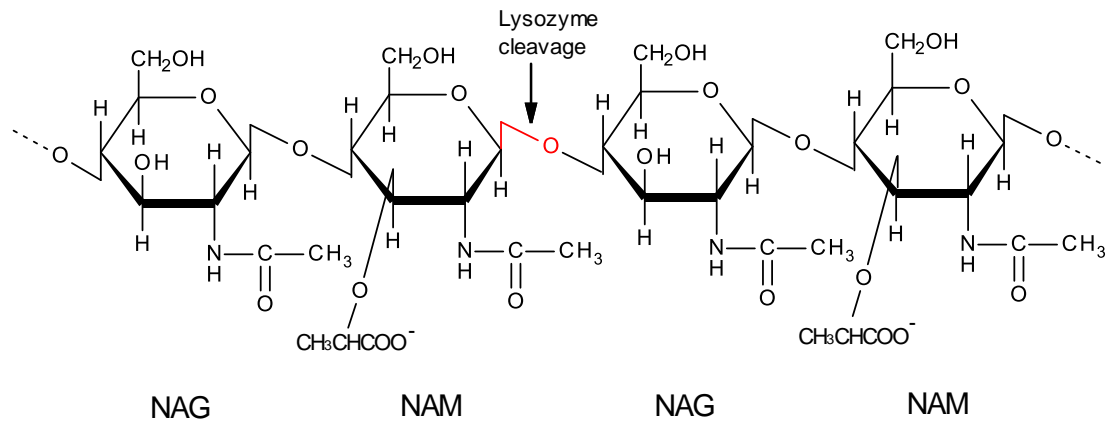


Figure 6. Lysozyme destroying bacteria cell walls by breaking $\beta(1-4)$ glycosidic bonds that lie in between NAM and NAG.

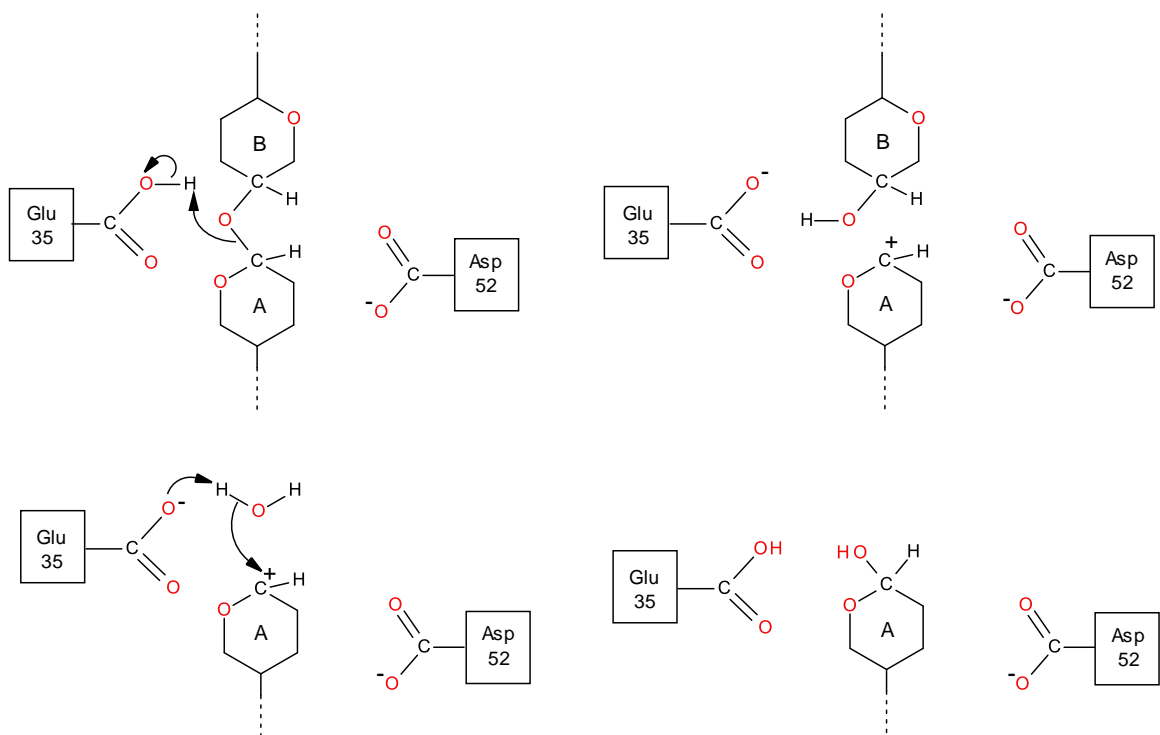


Figure 7. Lysozyme catalysis mechanism as established by Phillips in 1966.

The Philips mechanism (shown in figure 7) was established in 1966 ^[71] and occurs in a step-by-step process as detailed above. Initially, a strained conformation will occur when the residue becomes distorted which then allows the -CH₂OH group to interact with the enzyme. This step then results in the substrate acting as though it is in the transition state. The next step involves residue 35 which consists of glutamic acid and is highlighted as Glu35. Within Glu35 there is a proton which readily transfers to the polarised oxygen of the glycosidic bond and it is at this step where the C-O bond becomes cleaved. ^[72] The third step produces the intermediate oxonium ion because of the positive charge on residue A. The intermediate can either be produced by an aspartate residue, known as Asp52, acting as a negatively charged carboxylate and then reacting with the positively charged oxonium ion which results in a stability change. ^[73] The second method will rely on distortion of residue A allowing for resonance as the positive charge is shared between its carbon and oxygen atoms. The fourth step then involved residue B being released by the enzyme in conjunction with the polysaccharide producing a glycosyl-enzyme intermediate. The oxonium ion from the previous step will then react with H₂O from a solvent thus extracting the hydroxyl group to re-protonate Glu 35. The reaction completes by residue A being released alongside the polysaccharide. ^[74]

Koshland proposed two mechanisms for the hydrolysis of enzymatic glycosidic bonds. ^[75] The first is a retaining mechanism, where the glycosidic oxygen is protonated by acidic catalysts. Aglycon is released via nucleophilic reaction provided by a base. The resulting enzyme is hydrolysed via a H₂O nucleophilic substitution at the anomeric carbon. This gives it the equivalent stereochemistry to the substrate. The second is an inverting mechanism. The glycosidic oxygen is protonated and aglycon is released like previously, however there is an associated attack from a H₂O that is activated by the base residue. The product yielded has opposing stereochemistry compared to substrates because of this singular nucleophilic substitution. ^[76]

1.8 Nafion

Walther Grot first developed Nafion by altering a material named Teflon. Upon the discovery of Nafion (figure 8) a new group of polymers were created called ionomers due to a polymer having ionic properties for the first time. Sulfonic groups were added to the Teflon backbone in the polymer matrix, which gave the material an ionic characteristic. [77]

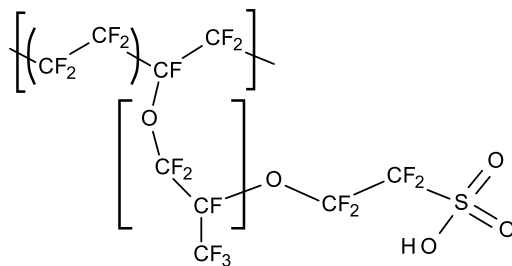


Figure 8. Molecular structure of Nafion

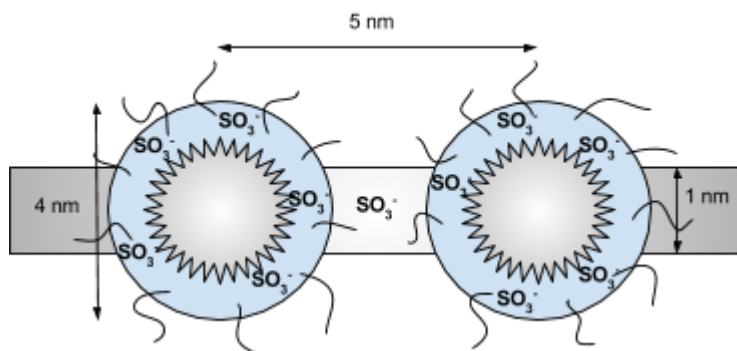


Figure 9. Clusters of sulfonate-ended perfluoroalkyl ether groups of Nafion [78]

Nafion has high resistance to damage made by chemicals because the bonding structure is very stable, which is due to the strength of the fluorine to carbon bonds. The structure in figure 8 shows how polymer units can be repeated within Nafion. [79]

When dry Nafion is covered by water droplets, the contact angles imply that the surface is hydrophobic. [80] This is shown by a study by Zhong *et al.* in which stainless steel was coated with Nafion and contact angles were measured confirming that the surface

would in fact appear hydrophobic. [78] However, over time it can be seen that Nafion does absorb water which therefore makes the material hydrophilic, so much so that it can be used as a drying agent. [80] There was also a report that signified anti-bacterial performance for the Nafion coated surface. Zhong *et al* suggested that the negative charge from the sulphonate groups (shown in figure 9) of Nafion reduce the adhesion of bacteria through repulsion against the negative charge from the bacteria cells. [78]

A study by Zhang *et al* [81] showed that varying the concentration of Nafion from 0.5 to 1 wt% changed the zeta potential from 0 to -12 mV which indicates that it has an overall negative net charge in these conditions.

Nafion is an ion-exchange membrane that has a range of applications. It can be used as a super acid catalyst in its acidic form. It can be used in electrolysis of water, production of chlor-alkali and recovery of metal-ions. Nafion can also be in proton exchange membranes for fuels. [82]

Due to the large size of the molecule that is created by polymerisation of monomers, there is a separation between polar and non-polar areas which provides a unique network for transportation of protons. The re-occurring feature of the models is the understanding that the hydration level determines the connections between ionic areas, which alters the dynamics of molecules of water as well as the movement of protons. [83]

Nafion is a self-assembling material that has the 'intelligence' to create regular matrix formations consisting of cavities that are linked by thin tunnels. Sulphonate (SO_3^-) groups cluster around the tunnels and cavities and there are exchanges with M^{2+} . This process acts in a similar way to proton exchanges in Langmuir monolayers. [84]

Despite the potential importance of materials such as Teflon and Nafion, there had been no nuclear magnetic resonance (NMR) data of these perfluorinated polymers in literature prior to 2001. The Schmidt-Rohr group gained the first spectra of ^{13}C high-resolution NMR for polymers of this type by combining rotation synchronised ^{19}F 180° pulses with 28-kHz magic-angle spinning (MAS). This data showed that the majority of Nafion backbones are formed in a helical fashion, even though Nafion is a random

copolymer. Disorder in terms of conformation occurs at the branched parts of the molecule. [85]

In addition to this, it was proved that a high number of chains in between branches rotate greater than 150° around the helix axis. The rigidity of the backbone is accounted for differently here than in other models that assume it is due to random coiling. [86]

The nanostructure that allows for the interesting properties of Nafion has now been identified through numerical fourier transformation. Novel approaches to this technique can determine quantitative analysis of scattering data with small angles. The resulting characteristics are as follows and are shown in figure 8. Long water packed channels arrange themselves randomly if not parallel and moderately hydrophilic side branches surround them (as shown in figure 10). This forms cylindrical inverted micelles, which are stabilised by the rigid backbone of polymer that is shown by NMR. When 20% of the volume is water, the average diameter for the water channels are 2.4 nm. Crystallites which are approximately 10% of the volume are stretched out and become parallel with the water channels, with a cross section of $\sim 5 \text{ nm}^2$. This model helps to explain imperative characteristics of Nafion such as quick diffusion of protons and water as well as its abilities at low temperatures. In addition to this, improved polymers that may be less expensive could be designed as a replacement to Nafion. [87]

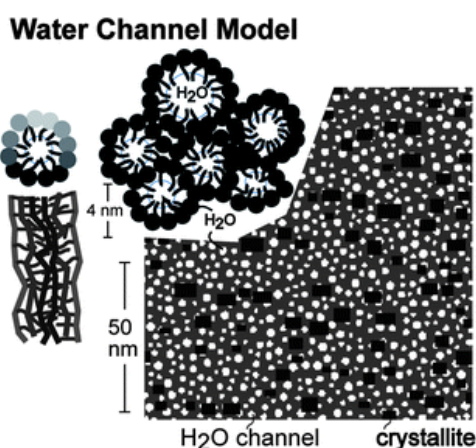


Figure 10. Nanostructure of Nafion [88]

1.9 Chitosan

Chitosan is a derivative of chitin and is a non-toxic and biodegradable polymer. [89] Chitosan can be obtained from crustacean exoskeletons [90] and is widely known for its antimicrobial properties. These antimicrobial properties could be due to its polycationic nature which means that it will react predominantly with anion components. [91] This reaction leads to leakage of the intracellular components of bacteria which in turn leads to cell death. [92]

The structure of the both chitosan and chitin is almost identical to the polymer cellulose (shown in figure 11). However, the hydroxyl group at carbon-2 is changed to an acetamide group. Chitosan is an N-deacetylated derivative of chitin because the acetamide groups are transformed into primary amino groups. [93]

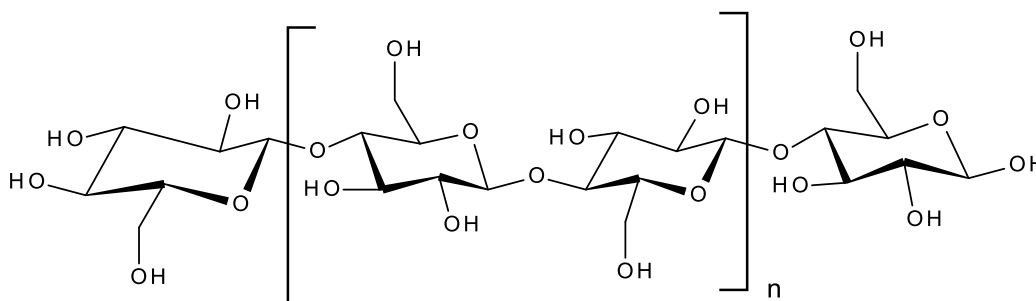


Figure 11. Molecular structure of cellulose

Both are polymers found in nature and are made up of β -(1,4)-linked D-glucosamine and N-acetyl-D-glucosamine units that are randomly distributed. [93]

The average degree of acetylation and how the acetyl groups are distributed throughout the chain are the main properties of solution. An irregular structure is given due to deacetylation because of the semi-crystalline characteristics of the polymer. [94]

The degree of ionisation depends on the pH and pK of the acid involved. This conclusion was based upon the protonation of chitosan in acetic acid and hydrochloric acid. [95] Chitosan that has a low degree of acetylation undergoes solubilisation at an average degree of ionisation of 0.5. This relates to a pH of 4.5-5. [96]

Chitin and chitosan have powerful antimicrobial properties that can be used to kill bacteria. Chitin is responsible for developing the serum in animals which contains antibodies. This acts as a defence mechanism against infection and disease. ^[97]

Evans *et al* conducted a test to show how capable chitosan is at gathering wide varieties of microbial cells together. They did this by testing how well chitosan binds to different types of microorganisms. ^[98]

The study showed that chitosan successfully lowered the levels of growth in microorganisms, meaning it bonded sufficiently to its target. *S. aureus* and *Klebsiella pneumoniae* were reduced as a result of the chitosan textile fibres. ^[99]

Chitosan also has its own derivatives such as chitosan glutamate and lactate. It was found that these showed aggressive antimicrobial properties towards *S. aureus*, *E. coli* and *Saccharomyces cerevisiae*. ^[100] It is also known that chitosan can be used in food preservation. Certain chitosan derivatives such as chito-oligosaccharide and various chitosan salts can be used, as well as chitosan that has low degrees of polymerisation. ^[101] The morphology of the structure of chitosan has been identified in literature. The electron diffraction diagram indicates an orthorhombic unit cell. The indexing of the unit cell ($P2_12_12_1$) where a is 0.807nm, b is 0.844nm and c is 1.034nm. The unit cell consists of two chains of chitosan that are antiparallel. No water molecules are present.

Solubility of chitosan can also be dependent on ionic concentrations. A salting-out effect occurs in excess of hydrochloric acid (1M) which means chlorhydrate forms of chitosan are able to be made. If the chlorhydrate form is in isolation, it is soluble in water. This gives a $pK_0=6\pm 0.1$ acidic solution, meaning it is soluble at pH lower than 6. ^[102]

This data agrees with work done by Domard *et al* in measurements of pH for acetylated chitosan. ^[103] In practical applications, the volume of acid needed is dependent on the amount of chitosan that needs to be dissolved. The concentration of $-NH_2$ units should be equalled or exceeded by the concentrations of protons. ^[104] To conclude, the solubility of chitosan is a difficult factor to have control over. Variables such as the degree of acetylation, ionic concentrations, protonation effect, pH and distributions of acetyl groups all affect solubility levels. ^[105]

It is important to fine tune these parameters to ensure as much of the chitosan is dissolved as possible for use in techniques such as (QCM-D).

Chitin (figure 12) and chitosan (figure 13) contain nitrogen groups which makes them able to react with amines. ^[106] The presence of primary and secondary hydroxyl groups on every unit makes chitosan more chemically active than chitin. ^[107]

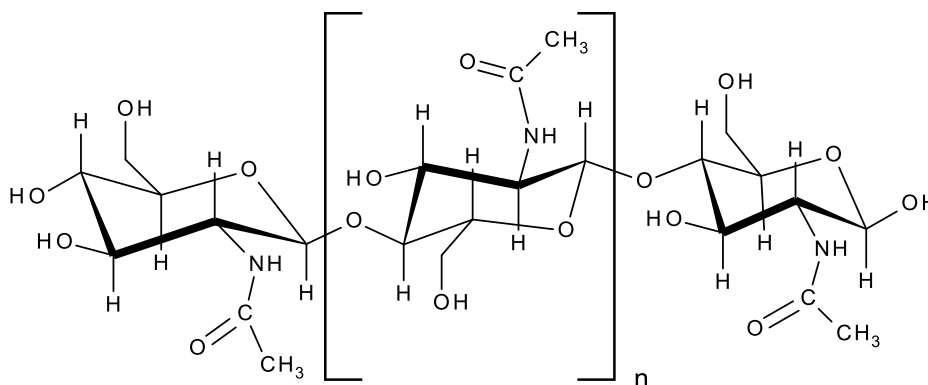


Figure 12. Molecular structure of chitin

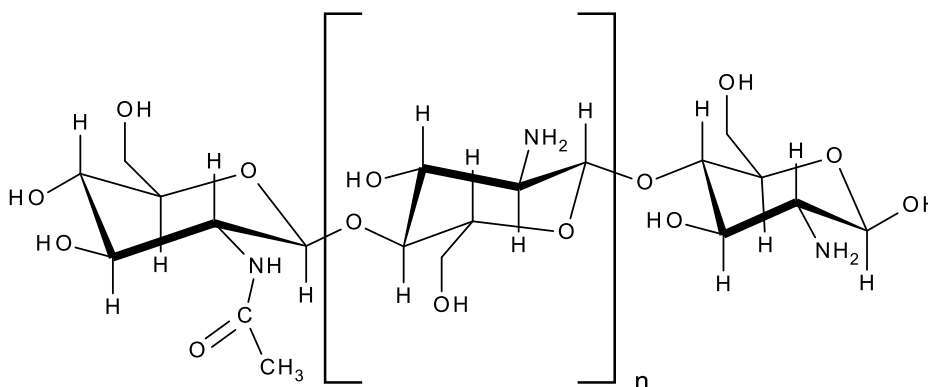


Figure 13. Molecular structure of chitosan

Chitin and chitosan are extracted from crustacean shell wastes and shrimp shells are the current most used biomass in industry to produce chitin and its derivatives. Chitin is extracted in a step-wise procedure by chemical methods. The shells are grounded into smaller parts and then hydrochloric acid is used to extract certain minerals. ^[108] Proteins in the residual materials are extracted with diluted sodium hydroxide (aq).

This forms Chitin which is deacetylated (in 40% NaOH at 160°C 2 hrs, absence of oxygen) which is then purified to give chitosan. ^[109] The process can be repeated to give higher deacetylation values up to 98%, but full deacetylation can never be completed without changing the process. ^[110] The concentration of NaOH, temperature used and time effects the level of transformation from chitin to chitosan. This procedure controls the amount of free amine groups (-NH₂) that are present in chitosan. ^[111]

Another method that could be used is chitosan in a water-soluble form where glycerol 2-phosphate is used at a neutral pH (between 7-7.1) and at room temperature. Temperatures above 40°C cause a gel to be formed which is only partially reversible. ^[112]

A study by Saïed *et al* stated that chitosan has an overall positive charge in acidic pH's ranging from 1 to 7. Also, the zeta potential values were highest at pH's less than 5 and fell significantly at pH's 6-7. ^[113]

2. Materials and Methodology

2.1 Materials

Nafion (CAS: 31175-20-9) *lysozyme* (CAS: 12650-88-3) *chitosan* (CAS: 9012-76-4) *sodium carbonate* (CAS: 497-19-8) *sodium bicarbonate* (CAS: 144-55-8) *citric acid* (CAS: 77-92-9) and Na_2HPO_4 (CAS: 7558-79-4) were all purchased from *sigmaldrich.co.uk* - based in Dorset, UK.

Nafion is readily dispersed in water ^[114] so this material is easily prepared for use in QCM-D. A solution of 1% Nafion in water was therefore prepared. Chitosan, as it is more difficult to disperse, needed to be dissolved in a solution containing acetic acid. A study by Saïed *et al* stated that chitosan at 0.1% concentration was soluble in 0.1% acetic acid solutions in water. This was the lowest concentration of acetic acid that would allow the chitosan to be dissolved and so this method was used to disperse the chitosan which produced a pH of 5. ^[113] A buffer solution can be used to resist a change in pH, even when small volumes of acid or alkali are put in the mixture. According to Sigma-Aldrich, Sodium carbonate-sodium bicarbonate and Citric Acid - Na_2HPO_4 can be used to produce buffer solutions of certain pH's. Buffer solutions of pH's 9, 7, 6.2 and 4 were created for 0.1% lysozyme solutions to make comparisons in data. The tables below show the necessary volumes of 'x' and 'y' needed to create these buffer solutions.

Table 2. Sodium Carbonate - Sodium Bicarbonate buffer solutions pH 8.8-10.8 ^[115]

pH		x ml 0.1M-	y ml 0.1M-
20°C	37°C	Na_2CO_3	Na_2CO_3
9.2	8.8	10	90
9.4	9.1	20	80
9.5	9.4	30	70
9.8	9.5	40	60
9.9	9.7	50	50
10.1	9.9	60	40
10.3	10.1	70	30
10.5	10.3	80	20
10.8	10.6	90	10

Table 3. Citric Acid - Na₂HPO₄ buffer solutions pH 2.6-7.6 ^[115]

pH	x ml 0.1M-Citric acid	y ml 0.1M-Na₂HPO₄
2.8	84.15	15.85
3.0	79.45	20.55
3.2	75.30	24.70
3.4	71.50	28.50
3.6	67.80	32.20
3.8	64.50	35.50
4.0	61.45	38.55
4.2	58.60	41.40
4.4	55.90	44.10
4.6	53.25	46.75
4.8	50.70	49.30
5.0	48.50	51.50
5.2	46.40	53.60
5.4	44.25	55.75
5.6	42.00	58.00
5.8	39.55	60.45
6.0	36.85	63.15
6.2	33.90	66.10
6.4	30.75	69.25
6.6	27.75	72.75
6.8	22.75	77.25
7.0	17.65	82.35
7.2	13.05	86.95
7.4	9.15	90.85
7.6	6.35	93.65

2.2 Methodology

The following methods were implemented to develop and assess the performance of the antimicrobial layers.

2.2.1 Quartz Crystal Microbalance with Dissipation Monitoring

Firstly, Q-Sense QCM-D was used to monitor the adhesion of the flowing phase to a substrate at a real time. The deposition of matter onto an oscillating crystal reduces its resonance frequency (f). The energy loss, otherwise known as dissipation factor (D), of the deposited ultrathin film is a measure of its rigidity and is also measured simultaneously^[116]. For LbL assembly, alternating layers of positively and negatively charged layers are deposited onto the crystal. The negatively charged particles were introduced to the system during the flowing phase and were then in contact with the crystal layer therefore allowing the deposition of a negatively charged layer. The next step was to wash off the weakly bounded particles via water rinsing. Subsequently, the positively charged particles are introduced as the flowing phase, following by water rinsing. The repetition of these steps creates a multilayer system.

QCM-D involves a crystal being used that is a piezoelectric material. This means an electrical field is formed when mechanical stress occurs, and the vice versa effect takes place also. When the potential (sine wave) is alternated, the crystal oscillates. The combination of a correctly cut crystal with a suitable alternating potential, gives a standing shear wave with the resonance frequencies of quartz.^[117]

The application of this technique can be used in surface chemistry. It is possible to determine the resonance frequency of quartz so when small volumes of material (ng/cm^2) are placed onto the crystals surface they can be quantified. This is done by calculating the change in resonating frequencies using the Sauerbrey equation as detailed below.

The QCM must be stabilised within ± 2 Hz.

The relationship between the frequency of QCM and mass can be estimated due to the adsorption of the QCM frequency shift. The Sauerbrey equation as follows shows the

relation between frequency shift, ΔF (Hz) and absorbed mass, M (g). A is the area of the crystal covered in material. [118]

$$\Delta F = -1.832 \times 10^8 M/A \quad (3)$$

Equation 2. Sauerbrey equation showing the relation between frequency shift, ΔF (Hz) and absorbed mass, M (g). A is the area of the crystal covered in material

The main advantage of this technique is its ability to measure the addition of materials layer by layer on a very small scale. It can measure surface to molecule interactions with nanogram precision when used alongside software called Q-sense. The build-up of the multi layers in a QCM-D system is highly reliable, while other techniques such as dipping typically suffer from a lower level of consistency.

Figure 14 shows what occurs to the sensogram QCM-D as mass is added. The adsorbed monolayer causes a drop in resonance frequency that is partially reversed after water rinsing. At the same time, dissipation is seen to increase first as expected due to the less rigid nature of the deposited layer compared to the crystal itself and then it partially reverses back upon rinsing.

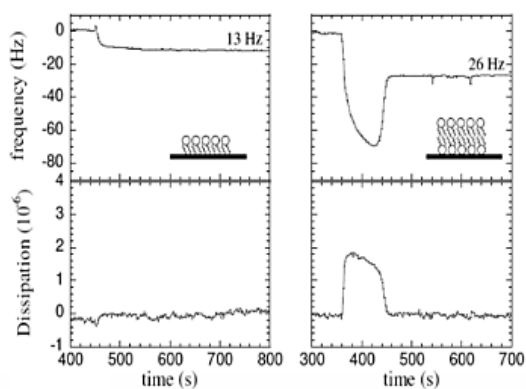


Figure 14. QCM-D sensogram showing the deposition of a lipid monolayer onto silica coated crystals [119]

2.2.2 Pre-coating of Gold Crystals

To create the first layer onto the crystal, the Ossila spin coating machine was used. A gold crystal was placed onto the machine and a small droplet of Nafion-ethanol solution was lowered onto the crystal. The machine separates the Nafion and ethanol, leaving a layer of Nafion deposited onto the crystal.

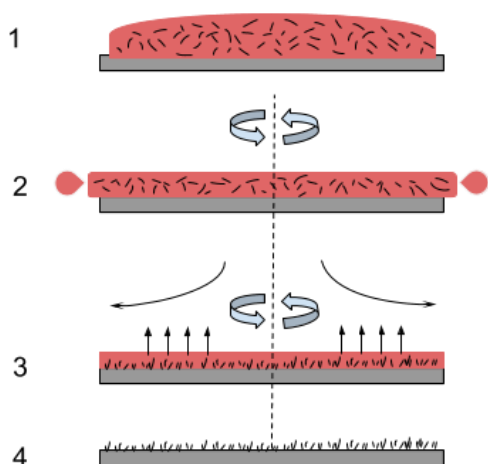


Figure 15. Step by step procedure for using the Ossila spin coating machine. ^[120]

The step by step procedure for spin coating is explained below and illustrated by figure 15. ^[120]

1. The gold crystal was coated with the solvent containing a mixture of Nafion and ethanol (1:40)
2. The crystal rotated at high speeds and most of the solvent was swept off the side
3. Airflow dries up most of the solvent which leaves a plasticised film
4. The film was left to dry and the desired molecules are left on the surface

The usual speed setting is 600 rotations per seconds. The surface tension in conjunction with the centripetal force drags the liquid state coating into an even coverage. At the same time the solvent is evaporated leaving the sought-after material.

Spin coatings have several advantages. Thin, uniform layered coatings can be created easily and the simplicity of the process is unmatched. High levels of consistency can be

achieved due to the high spinning speeds and high airflow, which applies at nano and macroscopic scales. ^[120]

One of the main disadvantages of this process is the lack of material efficiency as the process will only utilise between 2% and 5% of the material used. Also, there are increasing costs to both materials and waste material disposal. Despite this disadvantage, spin coating is most often the most highly regarded process for producing thin, uniform coatings. ^[121]

Nafion coated (monolayer) gold crystals were prepared in bulk. One crystal was then placed on the QCM-D chip and the sensor was initially exposed to distilled water at room temperature (22 ± 2 °C). The QCM-D crystals have gold-chrome electrodes that are 5mm in diameter and a surface area of 0.196 cm^2 . This gives a 9MHz fundamental resonance and the 3-micron finish gives a theoretical mass sensitivity of $5.458 \text{ ng Hz}^{-1} \text{ cm}^2$. The shear wave decay length is 250nm at room temperature. This is within the sensing region of the QCM-D to measure surface effects. ^[122]

2.2.3 Atomic Force Microscopy

Atomic force microscopy (AFM) is an imaging procedure where the apparatus used is a Digital Instruments Nanoscope (Scanning Probe Microscope). The AFM was set to contact mode where a sharp tip with a diameter typically between 5 and 10 nm is used to scan the surface providing information about its morphology. The method can also quantify the force of adhesion of an individual particle to the surface at which it is bonded to. This means that AFM can examine the surface roughness of an individual layer or a multilayer. ^[123] AFM has been proven to be the most appropriate method of measuring surface roughness on a glass-ceramic substrate due to the reduced risk of causing damage. ^[124]

2.2.4 Contact Angle Measurement

An OptoSigma optical tensiometer was used at room temperature to measure the contact angle and hydrophobicity of the surface coatings. A drop of distilled water was placed on the surface of the film and a video camera was used to record the change in shape. Software named 'FTA32' was used to analyse the image was used to measure the contact angle. The test was repeated several times to increase reliability. ^[125]

For surface coatings, a larger contact angle is more desirable as this means the surface is more hydrophobic and therefore the water will run off. Super-hydrophobic surfaces have a contact angle greater than 150° and show virtually no contact between the droplet and the surface, which would be the ideal scenario for surface coatings. ^[126]

2.2.5 Fourier Transform Infrared Spectroscopy (FT-IR)

An analytical method that will be used is Fourier Transform Infrared Spectroscopy (FT-IR). A Thermo Scientific Nicolet iS5 FT-IR was used. Firstly the sample was freeze dried, which was done by initially leaving it in a standard freezer for 2 hours and then moving the sample into the Scanvac Coolsafe freeze dryer to remove all water.

OMNIC Spectra Software was launched onto the computer desktop, the ZnSe crystal of the FT-IR was cleaned with acetone and a background test was collected. The freeze-dried sample was then placed onto the ZnSe crystal with a spatula and the knob is dialled until the sample is secured into the apparatus. When IR radiation is passed through a certain type of molecules, only frequencies that match the vibration frequencies of the molecules are absorbed. A 'fingerprint' of the data is collected and used to determine the samples chemical structure. ^[127] It can be used to assess purity by identifying the composition of base polymers, contaminants in organic materials and additives. More specifically, a variety of polymers can be used including, thin, soluble, liquids and irregular-shaped, which is ideal for this project. The absorbance spectra's shows the unique bonds and molecular structures of the layer that will be tested. ^[128]

2.2.6 Scanning Electron Microscope

A J-6000 scanning electron microscope (SEM) was used to produce high resolution, three dimensional images. The sample was initially freeze dried, as described early, and placed onto a sample holder. This was then placed in SEM and focused beams of electrons obtain information in order to form an image. The SEM focuses on surfaces as they can detect and analyse surface fractures and microstructures. This technique is an efficient way to observe the surface coatings to understand how the materials interact. ^[129]

2.2.7 Transparency Test

A UV-3600 UV-vis spectrometer and UVProbe 2.43 software was used to measure the attenuation of light after it has passed through the materials. ^[130] The materials were prepared by dipping the cuvette firstly in a 1% Nafion in water solution and leaving to dry, then dipping it in 0.1% lysozyme or chitosan solutions. When the layers dried sufficiently, the LbL surface coating formed was tested for absorbance to see how much light was absorbed when ultra-violet (UV) light is passed through. A blank cuvette was measured to use as a control.

2.2.8 Antimicrobial Activity Testing

This step was done in collaboration with the School of Pharmacy and Biomedical Sciences (PhD student Ella Gibbons), method adapted loosely from Zhong et al. ^[78]

Gold QCM discs, 1cm in diameter, were coated with a series of compounds (exact compounds and combinations listed in results section) via LbL. These discs, from here on referred to as test discs, were disinfected with isopropyl alcohol prior to each experiment as both autoclaving and UV sterilisation were unsuitable for the coatings. Two uncoated discs, referred to from here as control discs, were used in addition to the test discs in each experiment as means of providing a baseline for bacterial growth on the untreated discs. Due to being uncoated, the control discs were suitable for autoclave sterilisation.

For every experiment, each of the control and test discs were placed into separate wells in a flat bottomed 12 well plate. Each disc was placed atop a circle of autoclave sterilised

aluminium foil to prevent run-off of bacteria and to allow for easy transfer of the samples following their incubation.

Each disc was inoculated with 200µl of bacterial culture. The cultures themselves were grown in 25ml nutrient broth within 250ml Erlenmeyer flasks at 37°C for 24hrs. Following this overnight incubation, the cultures were transferred into 50ml Falcon tubes, balanced to within 0.1g of one another, and centrifuged at 4000rpm for 10 minutes. The supernatant from this centrifugation was then discarded of, 20ml of ¼ strength Ringer's solution added to each tube and the tubes vortexed to resuspend the pellet. The tubes were once again balanced and centrifuged at 4000rpm for a further 10 minutes. The supernatant, again, discarded of and this time 2ml of ¼ strength Ringer's added to each tube before vortexing. The resuspended cultures were then diluted by a factor of 100, via means of transferring 1ml culture into 9ml ¼ strength Ringer's twice.

Following inoculation, the 12 well plate was incubated for 20hrs at 37°C, after which the discs plus the foil were transferred into universal bottles, each containing 9.8ml Ringer's solution. These bottles were sonicated for 5 minutes and then diluted by a factor of 10 4 times, 100µl into 900µl each time. The dilutions were plated out in triplicate onto nutrient agar, spreading 100µl of culture onto each plate. The plates were then incubated for 24hrs at 37°C and subsequent growth recorded using a colony counter.

The test was conducted on two different bacteria. A gram-positive bacterium, *S. aureus*, and a gram-negative bacterium, *E. coli* was tested against various LbL assemblies. ^[131]

3. Results and Discussion

3.1 Precipitates

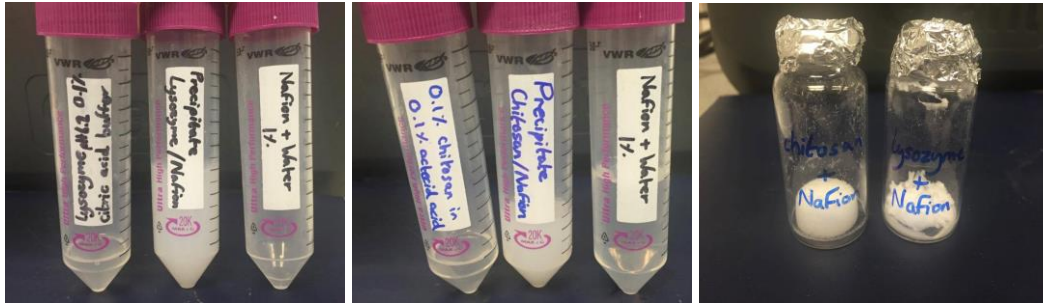


Figure 16. Precipitate of lysozyme (pH 6.2) and Nafion solutions, precipitate of chitosan (pH 5) and Nafion solutions and both precipitates post freeze dry (-76°C), from left to right.

Nafion and lysozyme solutions were mixed together to form a white precipitate (as shown in figure 16). The precipitate is a result of the negatively charged Nafion and positively charged lysozyme having electrostatic interactions. This occurred at when the lysozyme solution was at pH 9, 7, 6.2 and 4. Nafion and chitosan solutions were also mixed together to form white precipitates due to opposing electrostatic interactions.

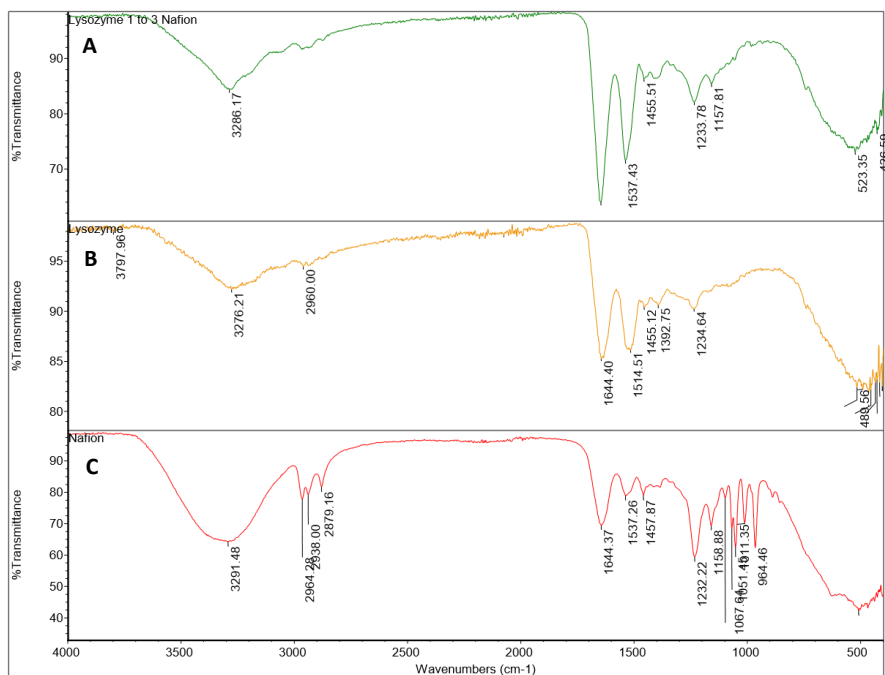


Figure 17. FT-IR spectroscopy data for (A) the precipitate of lysozyme and Nafion, (B) lysozyme and (C) Nafion.

Figure 17 indicates the following data. The FT-IR spectrum for lysozyme shows absorption bands at many points, these include bands at; 3276.21cm^{-1} which can be attributed to either an O-H stretch with hydrogen-bonding or an N-H group and 2960cm^{-1} which shows C-H bond stretches. There are bands at 1644.40cm^{-1} and 1234.64 also which could suggest the presence of an amide group as these wavelengths shows the bonds C=O and C-N respectively. There are also two bands; 1514.51cm^{-1} and 1455.12cm^{-1} , which show the presence of an aromatic C=C bond.

The spectrum for Nafion shows several absorption bands which confirm the presence of C-H groups, these wavelengths can be seen at 2879.16cm^{-1} , 2938.0cm^{-1} and 2964.28cm^{-1} . Also shown on the spectrum are absorption bands at 1011.35cm^{-1} , 1051.45cm^{-1} , 1058.88cm^{-1} and 1067.64cm^{-1} which are typical of ether groups, specifically C-O bonds. Other absorption bands depicted by the 1457.87cm^{-1} which shows C-H bending, 1537.26cm^{-1} which shows the presence of an aromatic C=C and 1644.37cm^{-1} which confirms the presence of an amide group with a C=O stretch typical to that seen within amides. The absorption bands shown on this spectrum are confirmed by the known structure of Nafion, which contains each of the bonds found.

The FT-IR spectrum for the combination of lysozyme and Nafion shows a characteristic blend between both molecules with no additional bonds being formed. The spectra for both lysozyme and Nafion confirm the presence of groups which will have electrostatic forces of attraction with each other and this will be the main form of interaction given that no permanent bonds have been formed.

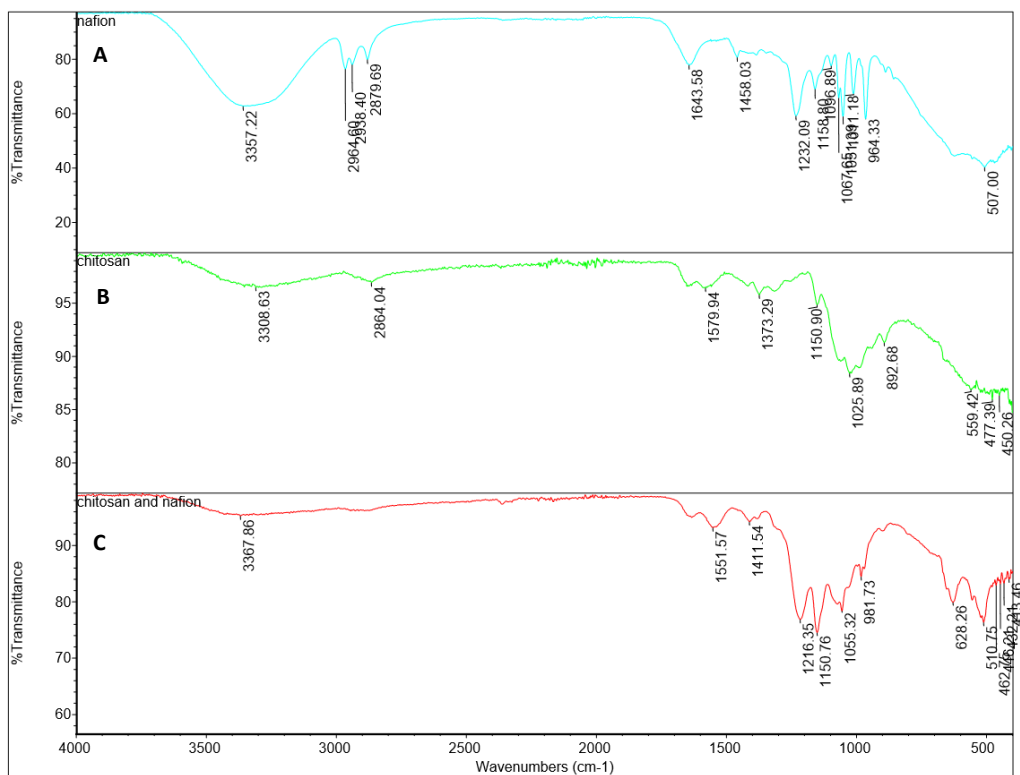


Figure 18. FT-IR spectroscopy data for (A) Nafion, (B) chitosan and (C) the precipitate of chitosan and Nafion.

Figure 18 indicates the following data. The FT-IR spectrum for Nafion confirms the presence of many groups. C-H stretch groups can be seen by three main peaks at 2879.69cm^{-1} , 2938.40cm^{-1} and 2964.60cm^{-1} . In addition to this there are 5 peaks which depict the presence of an ether group by the wavelengths 1011.18cm^{-1} , 1031.09cm^{-1} , 1067.65cm^{-1} , 1096.89cm^{-1} and 1158.80cm^{-1} which are all typical to the C-O bond within the ether group. Another group which was found by the spectrum was a C=O bond which is typically characteristic to that of an amide group. All the absorption bands shown on the spectrum correspond directly to the structure of Nafion which is known to contain each of these groups.

From the spectrum obtained for chitosan an absorption band of 3308.63cm^{-1} was measured, this could be indicative of either the amine bond N-H or an O-H bond with hydrogen bonding present. However, when taking intensity into account, it is more likely that this absorption band is relating to an N-H bond group. In addition to this, the

spectrum also confirms bonds such as C-O through the absorption band 1025.89cm^{-1} and further C-O groups which are shown by an absorption of 1150.90cm^{-1} .

Similarly, to lysozyme and Nafion, the spectrum for the combined materials show the characteristic bands of the parent molecules therefore confirming once again that no additional bonds have been formed. Instead, it can be concluded that it is likely that electrostatic forces are involved, such as hydrogen bonds being formed through the presence of -NH band present in chitosan and -OH band present in Nafion.

3.2 SEM

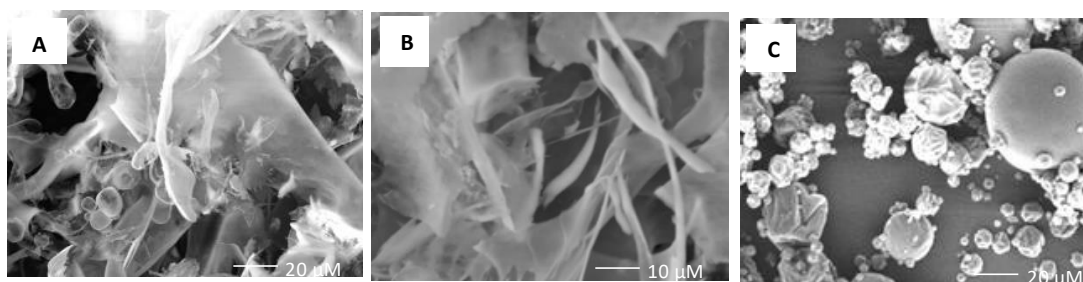


Figure 19. (A) SEM image of lysozyme and Nafion upon freeze dry measured at $20\ \mu\text{M}$. (B) SEM image of Nafion upon freeze dry measured at $10\ \mu\text{M}$ and (C) SEM image of clustering measured at lysozyme $20\ \mu\text{M}$ ^[132]

The images, in figure 19, above present the SEM results for when the precipitate of lysozyme and Nafion has undergone the freeze-drying process. These materials were mixed at a ratio of lysozyme 1:1 Nafion. Image A shows a general clustering of lysozyme molecules together around the long Nafion membrane. The clustering is reflected in C which is a clearer image. Image B shows the long string like morphology of Nafion which has been stated by Schmidt-Rohr ^[85] as long water-packed channels that arrange themselves either randomly or parallel with hydrophilic side chains around them. The clustering of lysozyme seems to occur more often near the long water channels of the Nafion as shown in image (A) of figure 19. This backs up data by FTIR and the production of the precipitate in that lysozyme and Nafion have electrostatic interactions.

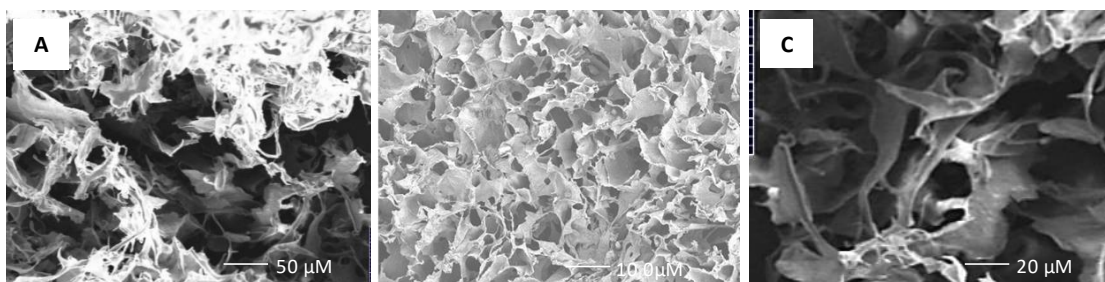


Figure 20. (A) SEM image of Nafion and chitosan precipitate upon freeze dry measured at 50 μM . (B) SEM image of the scaffold of chitosan measured at 100 μM ^[133] and (C) SEM image of Nafion and chitosan precipitate upon freeze dry measured at 20 μM .

Figure 20 presents images from the SEM for the precipitate of Nafion and chitosan that has undergone the freeze-drying process and were mixed at a ratio of 1:1. Image A shows the long water packed channels of Nafion but in a more random arrangement to previous images shown. Image B shows the scaffold structure of chitosan. Fernandes *et al* ^[134] stated that the average pore diameter of chitosan was 16 μM which gives 50% porosity. Image C shows a possible pore created by chitosan where nearby can Nafion water channels can be found. This backs up the formation of the white precipitate when the materials are mixed in solution and data found in FTIR that Nafion and chitosan have electrostatic interactions. Based on this information, these materials were used in QCM to build up LbL assemblies.

3.3 QCM-D

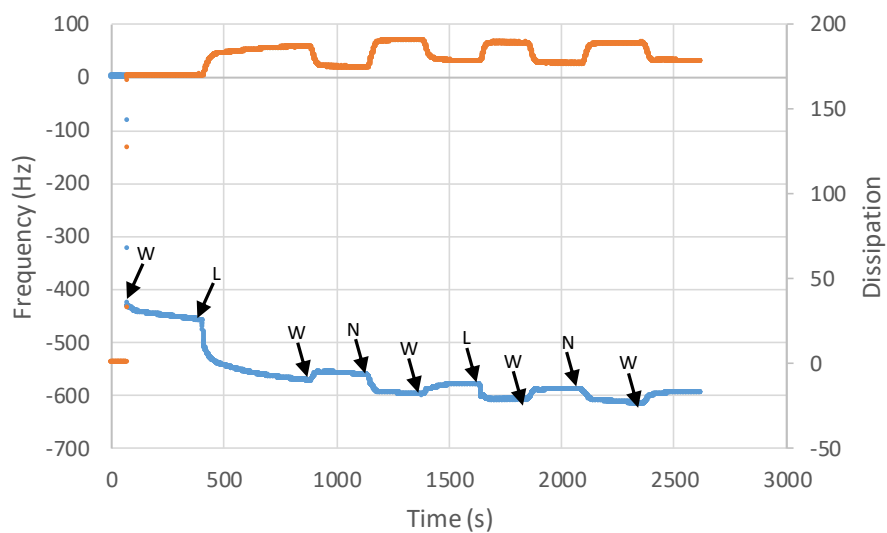


Figure 21. QCM-D sensogram during LbL deposition of Nafion and lysozyme (pH 9) onto a Nafion-coated crystal resonator with 2 layers of lysozyme and 2 layers of Nafion at room temperature (22°C). The frequency (f) is plotted in blue and the dissipation (D) is plotted in orange. “W”, “L” and “N” denote the injection of water, 0.1% lysozyme and 1% Nafion solutions respectively.

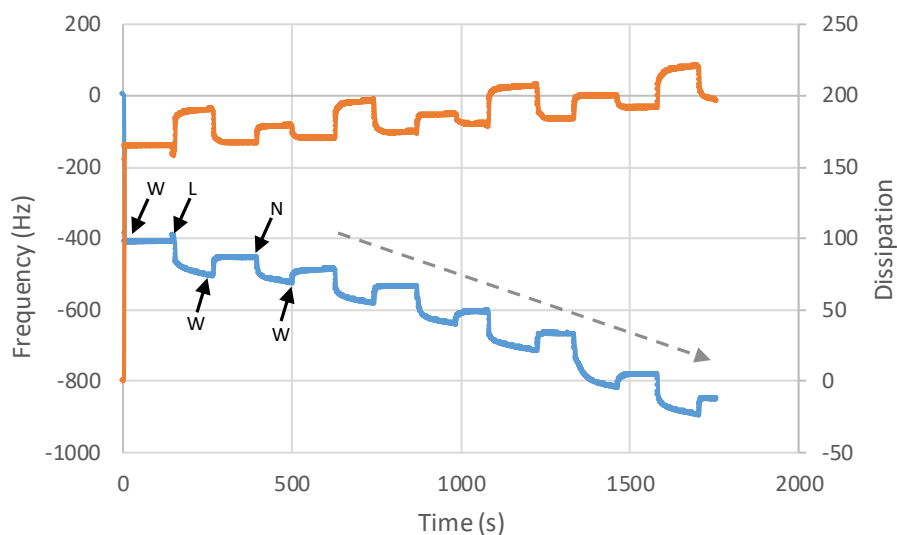


Figure 22. QCM-D sensogram during LbL deposition of Nafion and lysozyme (pH 7) onto a Nafion-coated crystal resonator with 4 layers of lysozyme and 3 layers of Nafion at room temperature (22°C). The frequency (f) is plotted in blue and the dissipation (D) is plotted in orange. “W”, “L” and “N” denote the injection of water, 0.1% lysozyme and 1% Nafion solutions respectively. The dotted line arrow represents the repeated steps of injections.

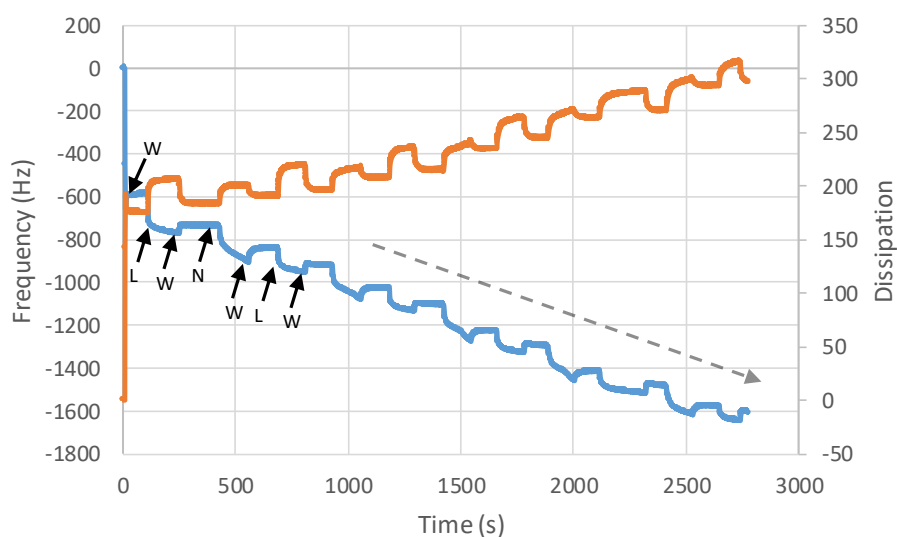


Figure 23. QCM-D sensogram during LbL deposition of Nafion and lysozyme (pH 6.2) onto a Nafion-coated crystal resonator with 6 layers of lysozyme and 5 layers of Nafion at room temperature (22°C). The frequency (f) is plotted in blue and the dissipation (D) is plotted in orange. “W”, “L” and “N” denote the injection of water, 0.1% lysozyme and 1% Nafion solutions respectively. The dotted line arrow represents the repeated steps of injections.

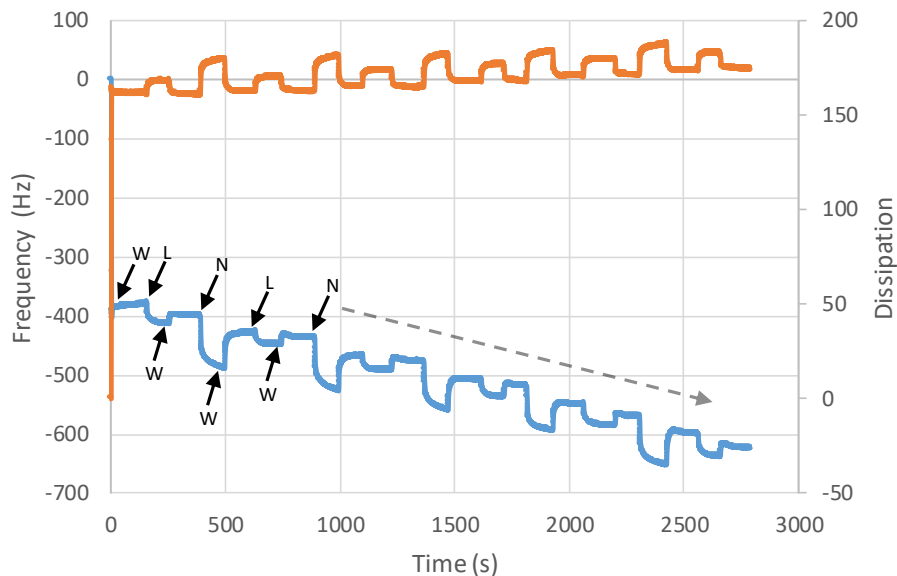


Figure 24. QCM-D sensogram during LbL deposition of Nafion and lysozyme (pH 4) onto a Nafion-coated crystal resonator with 6 layers of lysozyme and 5 layers of Nafion at room temperature (22°C). The frequency (f) is plotted in blue and the dissipation (D) is plotted in orange. “W”, “L” and “N” denote the injection of water, 0.1% lysozyme and 1% Nafion solutions respectively. The dotted line arrow represents the repeated steps of injections.

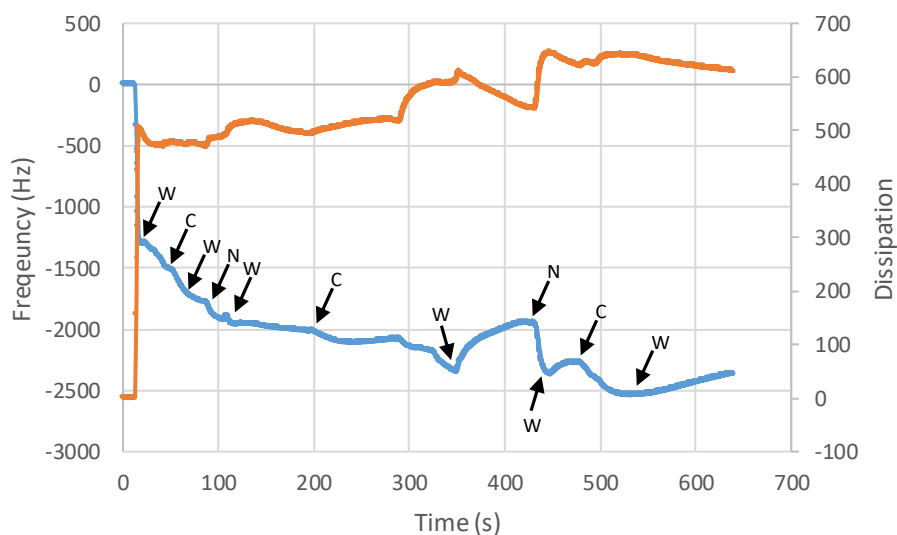


Figure 25. QCM-D sensogram during LbL deposition of Nafion and chitosan (pH 5) onto a Nafion-coated crystal resonator with 3 layers of chitosan and 2 layers of Nafion at room temperature (22°C). The frequency (f) is plotted in blue and the dissipation (D) is plotted in orange. “W”, “C” and “N” denote the injection of water, 0.1% chitosan and 1% Nafion solutions respectively.

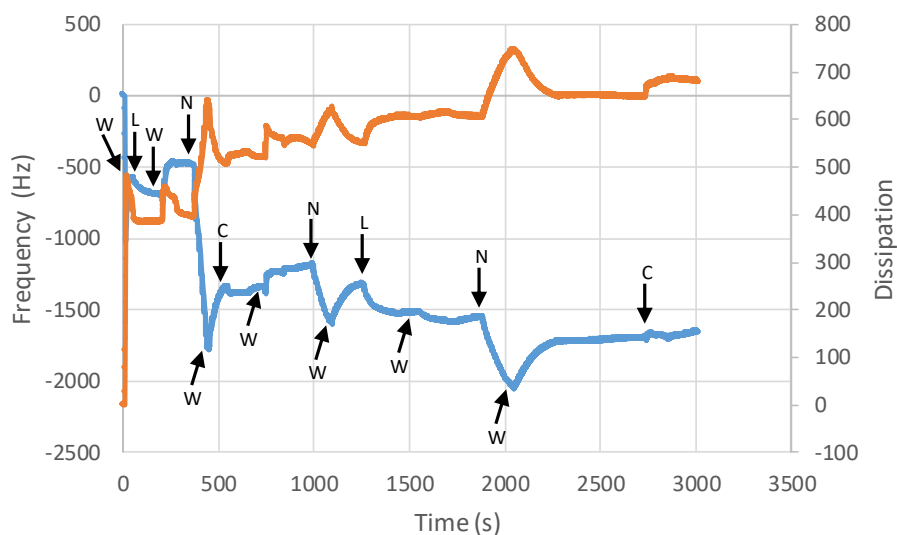


Figure 26. QCM-D sensogram during LbL deposition of Nafion, chitosan (pH 5) and lysozyme (pH 7) onto a Nafion-coated crystal resonator with 2 layers of chitosan, 2 layers of lysozyme and 3 layers of Nafion at room temperature (22°C). The frequency (f) is plotted in blue and the dissipation (D) is plotted in orange. “W”, “C”, “L” and “N” denote the injection of water, 0.1% chitosan, 0.1% lysozyme and 1% Nafion solutions respectively.

Figures 21-24 show the QCM-D data collected and repeats of these tests can be found in the supplementary data. For figures 25 and 26, QCM-D data was collected once, therefore no repeats for these are provided within supplementary data.

Figure 21 shows the QCM-D data of a 0.1% lysozyme in sodium carbonate-sodium bicarbonate buffer solution and 1% Nafion in water with gold crystals pre-coated with Nafion and ethanol at a ratio of 1:40. 3.5 bilayers of Nafion/lysozyme (pH=9) were created.

The frequency (f) is a measure of the oscillations of the quartz crystal as mass is added to the sensor. Dissipation (D) is a result of the lapse in energy when the voltage towards the crystal is stopped.

At 20s, the frequency signal drops to -450Hz. This initial drop is caused by the water molecules either entrapping within in the Nafion monolayer or by direct hydration.^[135] The amount of water adsorbing onto the surface ultimately depends upon its orientation of either ‘side-on’ or ‘end-on’ as more water will be present should they adsorb in the ‘end-on’ orientation.^[67]

The frequency drop upon addition of water falls within a range consistent with a study by Fernandes *et al.* [136]

The first layer of lysozyme adsorbs sufficiently onto the surface of the Nafion with the frequency dropping from -450Hz to -570Hz. Then subsequent lysozyme layers show differences of 20-30Hz. The layers of Nafion causes frequency changes of around 20-30Hz also. The Sauerbrey equation can be used to describe the frequency to mass relationship at the surface of the crystal.

The trends in terms of dissipation and frequency are consistent throughout the results. From the graph, it is clear when a new layer is added and when the excess is washed off with water. The results from the other Nafion/lysozyme (pH=9) results show consistency and can be found in the supplementary data. The reliability of the repeats means that these QCM-D data are easily reproducible when using the buffer of pH 9.

There are currently no published journals that have explored the idea of building a LbL system consisting of Nafion and lysozyme and therefore this research is novel. Nafion has an overall negative charge because the polymer molecule has at least one excess electron at a time. [137]

Lysozyme at a pH below 11 has an overall positive net charge, which is shown in a study by Dolinsky *et al* where it is concluded that as the pH becomes more acidic there is a higher positive charge value. [138]

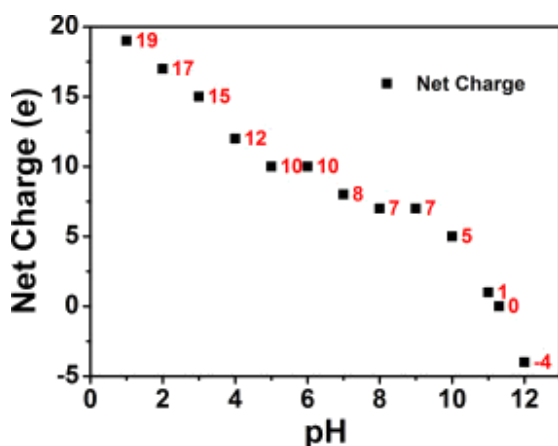


Figure 27. pH changes influence the net charge of lysozyme [139]

Changes in the pH of the lysozyme with the use of buffers could potentially give different frequency and dissipation levels in the QCM-D system.

Figure 22 shows the data for when 4 bilayers of Nafion/lysozyme (pH=7) were created. The initial frequency as water is added is as expected. The changes in frequency for both lysozyme and Nafion layers added are in conjunction with the data that Dolinsky et al presented, as the addition of Nafion layers show larger changes in frequency than 3.5 bilayers of Nafion/lysozyme (pH=9). It is likely that when there is a more positive charge, the molecules of the proceeding Nafion layer will more readily be attracted the lysozyme and form more electrostatic interactions. However, in comparison to the 6 bilayers of Nafion/lysozyme (pH=4) data there is not much difference in the change of frequency per Nafion layer.

A study by Araki *et al* stated that the adsorption of lysozyme onto a gold crystal was pH insensitive. However, as a multilayer system is being created here, it would appear the interactions between layers is dependent on the charges that the varying pH's create. Araki et al explained that even if lysozyme was pH insensitive, the dissipation results showed a softness of the adlayer created. This could affect the interactions between layers in LbL system where a stiffer layer of lysozyme would encourage molecules of the proceeding layer to be added by electrostatic interaction. ^[140]

A buffer was made at the optimal pH for lysozyme to be most active at. At pH 6.2, lysozyme shows the most activity over a larger ionic strength range. ^[141]

Figure 23 shows the QCM-D data for 6 bilayers of Nafion/lysozyme (pH=6.2). Lysozyme is most active at pH 6.2 due to a higher activity over a larger ionic strength range. The adhesion of the layers to the surface is similar to that in the 4 bilayers of Nafion/lysozyme (pH=7) data. The change in frequency when Nafion is added is also similar to the 4 bilayers of Nafion/lysozyme (pH=7) results but is more consistently around 100Hz which follows Dolinsky's findings.

The trends of the results are consistent and so are reproducible. It appears that when water is used to wash the excess off, less material is lost in comparison to when other pH's were used. This could either be due to a difference in rigidity of the layers formed or the levels of water entrapment within the layer are higher.

Figure 24 shows the data for when 6 bilayers of Nafion/lysozyme (pH=4) were created. The frequency of the initial addition of water is slightly lower than usual, which is possibly due to less Nafion molecules being adsorbed to the surface during the spin coating process. As the layers of lysozyme are added, the frequency changes by approximately 20Hz each time, which is significantly less than when compared to the 4 bilayers of Nafion/lysozyme (pH=7) and 5 bilayers of Nafion/lysozyme (pH=6.2) data.

When Nafion is added the frequency drops around 90-100Hz. This follows the statement made by Dolinsky *et al* that the lower the pH, the higher the net charge. It can also be seen that as each layer of Nafion is added, there is around a 50% decrease in adsorbed material as the excess is washed with water. This suggests that layer of Nafion is not strongly bonded despite the higher electrostatic forces.

Figure 25 represents the data for when 3 bilayers of Nafion/chitosan (pH=5) were created. Unlike the results prior to this there is no repeatable trend where the layers have been adsorbed and washed off, however it is still clear that adhesion has occurred. The initial addition of water to the QCM-D changed the frequency outside of the usual range of -450 to -550 Hz. This could have been due to impurities in the water or human error in the coating of Nafion for the first layer. As the test continues, the changes in frequency still show that chitosan and Nafion were successfully added as a LbL system. There was a substantial change around 350s which indicated vast amounts of material were washed off. The subsequent layer however had high adhesion, which means that there was no issue with the polarity of the previous layer despite losing large mass.

The overall frequency changed to around -2400Hz, which indicates large masses of material added. However, the repeatability of this LbL construct is more difficult than the lysozyme/Nafion constructs as shown by the lack of trends. A likely reason for this is that the chitosan is not uniformly distributed across the layer when added which could be due to specific requirements when dispersing chitosan.

Figure 26 shows that a LbL system can be created that contains all materials lysozyme, Nafion and chitosan. The data presents the QCM-D data for 4 layers of Nafion, 2 layers of chitosan and 2 layers of lysozyme (pH=7). The theory behind this is that the assembly

is built upon the alternations between Nafion – lysozyme – Nafion – chitosan and repeated this way, maintaining the principle of alternating opposite charges.

The data is less reliable than other data presented as there is no obvious patterns or trends to follow. However, it is clear to see that there is adhesion of Nafion layers around 400s, 1000s and 1800s. The change in frequency and dissipation for the adhesion of Nafion here is a lot larger than in previous results despite no obvious changes within the method.

It is possible that there are more random arrangements and orientations of molecules because of the introduction of a third material. The changes in frequency for the addition of the lysozyme and chitosan are minimal which again indicates a lack of reproducibility. This could be due to repulsion between the two layers of positively charged lysozyme and chitosan molecules which encase each Nafion layer. For example, if a layer of lysozyme does not cover the Nafion with a full monolayer, when chitosan is used, the positive charges will repel.

3.4 AFM

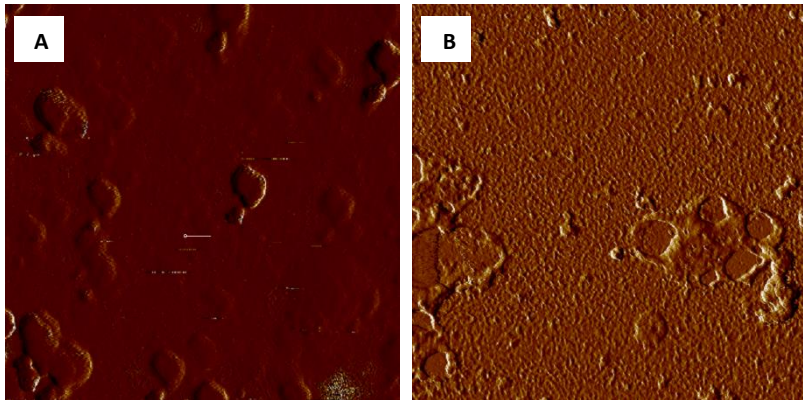


Figure 28. AFM images of Nafion and lysozyme (pH 9) LbL assembly (A) and (B) from left to right.

AFM studies of lysozyme-Nafion were carried out to investigate the cluster formations found in SEM and other information about the LbL formation. Figure 28 images A and B shows the surface of 3.5 bilayers of Nafion/lysozyme (pH=9), which was the only LbL construction tested. The roughness average (R_a) of image A is 5.70nm, which is the arithmetic mean of the height of the surface, position and length. When this is compared to R_a of image B, which is 4.18nm, there is a difference of 1.52nm. As the images are both of the same batch of material (but different areas) this could suggest that the spread of roughness is fairly even, but it does deviate.

The root mean square of roughness (R_q) is another measurement that can be used. The advantage that R_q has over R_a is that it is more sensitive to peaks and troughs in the average roughness of the surface because the amplitude is squared. The R_q of figure A is 29.1nm whereas figure B is 6.79nm. This shows that the surface in two different areas has large changes in roughness indicating that the size of the peaks and troughs vary substantially throughout the surface.

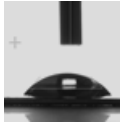
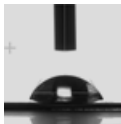
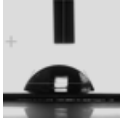
The maximum profile peak (R_{max}) measures the highest point of the surface from the baseline. The R_{max} of image A is 1888nm which is much greater than any of the averages. This peak could indicate a crack in the surface, which is important to consider when comparing against other figures. The R_{max} of image B is 75.9nm which is more realistically of a peak that larger than the rest but is not an anomaly. ^[142]

It has been suggested that lysozyme adsorbs onto the surface as monomers and the proteins diffuse forming clusters. Protein monomers do not land on top of previously adsorbed proteins which is probably a result of electrostatic repulsions. They move laterally and adhere next to the monomer, increasing the growth of clusters. Several other studies also confirm that proteins in aqueous state diffuse onto solid surfaces. [143][144][145]

If there is a sufficient protein content in a lysozyme solution, there will be initial clusters formed, then proteins adsorb to create a complete monolayer, and then multilayers will be formed. It is expected that it takes a longer amount of time for the additional layers to form compared to the time it takes for a monolayer to form. Despite this, all lysozyme layers are irreversibly adsorbed. Kim argued that the proteins can undergo conformational changes such as unravelling to assist in multilayer formations. Diffusion at the surface and collisions of neighbour proteins allows for the aggregation of the surface. ^[146] The clustering formation phenomenon is captured by the AFM when the surface is only sparsely populated.

3.5 Contact Angle Measurements

Table 4. Contact angles of the various LbL assemblies at different pH's

Surface	pH	Contact Angle (°)	
Lysozyme and Nafion	4 (6 bilayers)	45.35	
	6.2 (6 bilayers)	55.95	
	7 (4 bilayers)	58.63	
	9 (3.5 bilayers)	59.38	
Chitosan and Nafion	5 (3 bilayers)	60.76	
Lysozyme, chitosan and Nafion	-	42.21	

Contact angle measurements reflect the interplay between the chemistry of surface groups and the surface topology of the coatings. Table 4 shows the contact angle behaviour of the various materials. The contact angle of the lysozyme and Nafion layers increases as the pH increases. Repeated contact angles can be found in supplementary data.

These results are coherent with a study conducted by Vasani *et al* where the contact angle of porous silicon (pSi) and poly(2-diethylaminoethyl acrylate) films (pSi-pDEAEA) increases as the pH increases. The theory behind these results can be applied to both sets of data. When the pH is higher than the pKa value, intramolecular hydrogen bonds are formed due to the deprotonation of amine groups in the surface, which makes the surface hydrophobic. This explains the results that occur for 3.5 bilayers of Nafion/lysozyme (pH=9) which gave a contact angle of 59.38° in comparison to 6 bilayers of Nafion/lysozyme (pH=4) which gave a contact angle of 45.35° – a larger amount of amine groups become deprotonated making it more hydrophobic. Due to lysozyme containing many amino acids that contain amine groups, this theory can be applied.^[147]

Table 5. pK_a of acidic residues in chicken egg white lysozyme at 35° C^[148]

Residue	pKa
	Alpha
Glu 7	2.7
Asp 18	2.3
Glu 35	6.1
Asp 48	2.3
Asp 52	3.6
Asp 66	< 2
Asp 87	2.3
Asp 101	4.0
Asp 119	3.1
C-terminal	3.1

Table 5 presents the pKa values of acidic residues in chicken egg white lysozyme. This data backs up the points made previously that when the pH value is higher than the pKa, the surface is more hydrophobic because most of these values are below 4.0. The residue 'Glu 35' has the highest pKa value which is markedly similar to the most active pH of lysozyme (6.2). Due to the importance of Glu 35 in the catalysis in lysozyme molecules its activity should be an important marker in deciding the most appropriate pH to use for this surface coating in terms of LbL assembly, antimicrobial activity and contact angles.

The 3 bilayers of Nafion/chitosan (pH=5) surface coating had the largest contact angle of 60.76° which is similar to results in a study by Kim *et al* where the contact angle for pure chitosan was 56.90°. ^[149]

The difference in contact angle between the 3 bilayers of Nafion/chitosan (pH=5) surface coating and the 3.5 bilayers of Nafion/lysozyme (pH=9) coating was minimal, however still significant as it means the Nafion/chitosan surface is more hydrophobic than the others. This includes the contact angle for LbL assembly with 4 layers of Nafion, 2 layers of chitosan and 2 layers of lysozyme (pH=7) which accounted for the second lowest contact angle of all the results. An explanation for this result could be that there is an increased random arrangement and orientation of molecules as suggested in the QCM-D results section.

Wenzel defined the relationship between wettability and surface roughness stating that an increased surface roughness enhances the wettability of a surface. ^[150]

Thus, the roughness affects the contact angle measurements. From the AFM results it can be said that the surface coatings have a significant number of peaks and troughs which could be the reason for the low hydrophobicity. This means the surface coating will not easily allow water to just run off the surface which would be ideal for an antimicrobial surface coating. This should be a focus of future work in this area.

3.6 Antimicrobial Activity

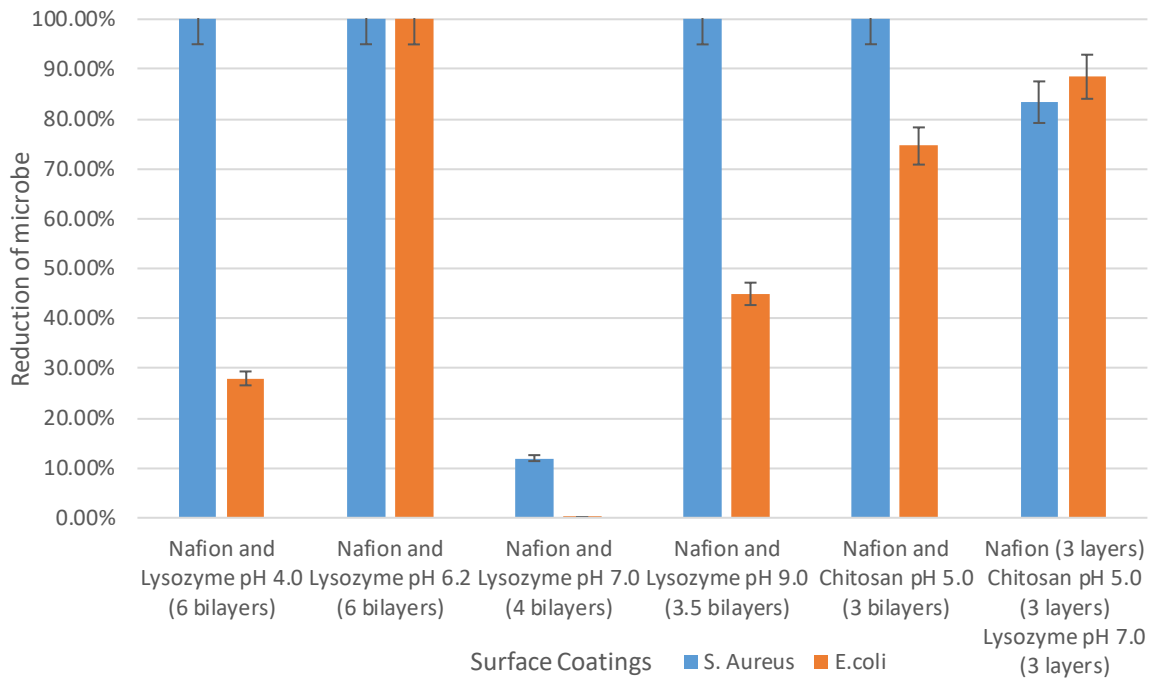


Figure 29. Percentage reduction of *S. aureus* and *E. coli* for various LBL assemblies

Figure 29 represents the data collected from the antimicrobial tests. The antimicrobial tests were carried out for each LBL construction in the presence of either *S.aureus* or *E.coli* and the tests were carried out once in each instance. These results were completed in collaboration with Ella Gibbons of the School of Pharmacy and Biomedical Sciences.

It is essential that *E. coli* and *S. aureus* are controlled in a safe manner as these microbes are the most common occurrences in outbreaks of foodborne disease.^[151]

The surface coatings produced are an attempt at combatting this problem. Varying pH's of lysozyme were created and used with Nafion to see which was most effective. In addition, Nafion was used with chitosan (pH=5) and a final assembly consisting of lysozyme, Nafion and chitosan was also created in the QCM-D.

The results show us that the 6 bilayers of Nafion/lysozyme (pH=6.2) assembly is the most effective pH in terms of destroying both strains of bacteria. More than 99.9% of

S. aureus and 99.9% of *E. coli* were reduced, which is expected at pH 6.2 because, as Davies et al wrote, the maximum activity of lysozyme is observed at this pH. ^[141]

The 6 bilayers of Nafion/lysozyme (pH=4) and 3.5 bilayers of Nafion/lysozyme (pH=9) tests proved to work well against *S. aureus* (>99.9% and 99.9% respectively) however did not reduce as much *E. coli* as the former (28.0% and 45.0%). The coating of 4 bilayers of Nafion/lysozyme (pH=7) decreased *S. aureus* by 12.0% and *E. coli* by ~0%. The 6 bilayers of Nafion/lysozyme (pH=4), 6 bilayers of Nafion/lysozyme (pH=6.2), and 4 bilayers of Nafion/lysozyme (pH=7) results are in accordance to the results of a study by Wecke et al, who stated that despite previous findings, lysozyme can attack cell walls of *S. aureus* when used in acidic conditions, as the 6 bilayers of Nafion/lysozyme (pH=4) and 6 bilayers of Nafion/lysozyme (pH=6.2) results were more effective than the 4 bilayers of Nafion/lysozyme (pH=7) result.

Wecke et al ^[152] stated that under acidic conditions, a new attacking mechanism occurs from the inside of the cell wall. Studies with an electron microscope showed that the attack started within the cross-wall and lytic sites become arranged between the cell wall and cytoplasm membrane, causing a gap to form and wall segments becoming trapped in the medium. The 3.5 bilayers of Nafion/lysozyme (pH=9) results do not follow this trend because it is not under acidic conditions. However, this result could also be due to Nafion being the last layer to be added to the LbL system (shown in the QCM-D data). This is crucial as the top layer of the LbL assembly is more exposed to the microbes than other layers. Preliminary data from our lab stated that Nafion on its own had antimicrobial activity which could explain the 3.5 bilayers of Nafion/lysozyme (pH=9) result. ^[153]

The 3 bilayers of Nafion/chitosan (pH=5) LbL construct also showed high-levels in reduction of *S. aureus* (>99.9%) and *E. coli* (74.6%). This behaviour is consistent with the with the well- explored antimicrobial activity of chitosan against the bacteria tested here. ^[154]

The LbL system consisting of 4 layers of Nafion, 2 layers of chitosan and 2 layers of lysozyme (pH=7) decreased *S. aureus* by 83.4% and *E. coli* by 88.5%. Again, high levels of reduction are exhibited due to the materials used.

Despite the observations made by the results, there are some limitations that should be considered. A possible limitation is in the event that the crystals weren't washed with water after the last layer of material was added in the QCM-D machine. The excess material which could be left on the crystals could dry and then produce deviations in results, particularly because the antimicrobial testing comes into contact with the top layer first. Another factor that could influence the results is the number of layers that are used in each test, where it would be assumed that if more material is built in the LbL assembly it would have higher antimicrobial activity. However, the 4 bilayers of Nafion/lysozyme (pH=7) test has more layers than the 3.5 bilayers of Nafion/lysozyme (pH=9) test and less antimicrobial activity so this point is subjective.



Figure 30. Antimicrobial effect of gold crystals, upon which the LbL systems were formed, against *S. aureus* and *E. coli*

3.7 Transparency Test

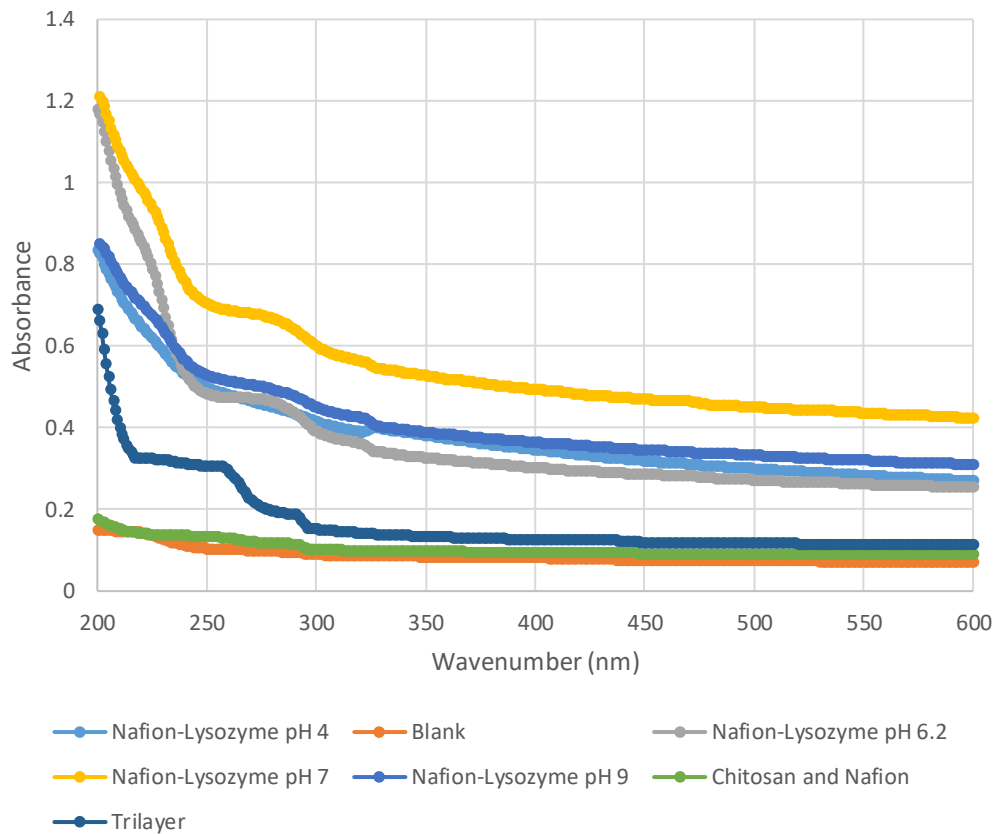


Figure 31. Comparison of absorbance of a range of dipped LbL assemblies

Figure 31 shows the comparisons of absorbance for all the materials. The materials were prepared by dipping the cuvette firstly in a 1% Nafion in water solution and leaving to dry, then dipping it in 0.1% lysozyme or chitosan solutions. When the layers are dried sufficiently, the surface coating formed consists of one layer of each component. The coated cuvettes were then tested for absorbance to see how much light is absorbed when ultra-violet (UV) light is passed through. A blank cuvette was measured to use as a control. This was not repeated and so results are based on the initial transparency test carried out.

Proteins such as lysozyme absorb UV light at peaks 280nm and 200nm. The peak at 280nm is a result of aromatic rings and amino acids (due mostly to the presence of tyrosine and tryptophan) which are present. The peak at 200nm is present due to the peptide bonds. The absorbance spectrum can be affected by the structure of the

protein whether it be secondary, tertiary or quaternary. In addition to the structure having an impact, pH and ionic strength can also alter the absorbance spectrum. ^{[155][156]}

The absorbance for Nafion is at 228nm and this is seen in the change in wavelength, however it is not as present as the lysozyme protein peaks, suggesting that the dipping technique adheres more lysozyme than Nafion. ^[157]

The Nafion/chitosan assembly shows results that correspond with the UV-vis given by Kumirska et al for chitosan and a derivative. This could suggest that the LbL assembly here had larger amounts of chitosan than Nafion. The system that contained lysozyme, Nafion and chitosan showed an absorbance of all of three materials as expected. ^[158]

The results show that the more neutral the pH is, the higher the absorbance is. This is in accordance with the results of a study by Nagasaka *et al* ^[159], where LbL films of fluorescein-modified poly(allylamine) (F-PAH) and poly(styrenesulfonic) (PSS) layers were alternately deposited through electrostatic forces of attraction. Nagasaka *et al* wrote that absorbances of the film were higher at more neutral pH's than in weakly acidic solutions.

The definition of transparency is the property of allowing light to pass through so that objects behind can be seen. The absorbance of light measured here can be an indicator of the amount of light that is stopped by the material and so it is possible to compare these results. Figure 31 shows that there is minimal to no peaks in the visible wavelength spectrum (400-800nm). This is a positive result as this means the LbL materials that were deposited on the cuvette have no visible colour to them. Consequently, if these materials are applied to materials such as tin foil (to protect food) or door handles, they would have minimal to no visible colours which is a property of an ideal antimicrobial surface coating.

Aside from the blank control, the Nafion/chitosan assembly had the lowest absorption which suggests that it is less visible than the other coatings. This was followed by the assembly with lysozyme, chitosan and Nafion which was unexpected as the thickness and opacity of this material should have been increased due to the increased number of materials used. The pH 9 and pH 4 lysozyme-Nafion assemblies had similar

absorbance and as stated previously the more neutral pH's have the highest absorbance.

This approach to measuring absorbance of light/transparency is limited however, as the drying process of the cuvettes could create clouding effects from the layers deposited, and the thickness of the layers should be more reproducible. Also, some of the material may get scratched off as it is placed inside the UV-vis machine.

4. Summary

We investigated for the first time the development of LbL materials comprising of Nafion and lysozyme. Preliminary data in our lab demonstrated that Nafion shows antimicrobial activity in line with the well-explored antimicrobial behaviour of lysozyme.

Using QCM-D sensograms, stable LbL ultrathin coatings based on Nafion and lysozyme (pH 9, 7, 6.2 and 4) were formed. Judging from the magnitude of the frequency drop (that is a measure of the total mass deposited on the crystal) observed after the deposition of Nafion, it is clear that Nafion adsorption on the lysozyme monolayer is systemically stronger as the pH of lysozyme decreases. The changes in pH also effected changes of frequency when lysozyme was added. It could be concluded that the more neutral pH's exhibited higher frequency changes for lysozyme (and therefore more mass).

Nafion and chitosan LbL assemblies were also chosen to be constructed based off the principle that building units have opposing charges and the formation of a white precipitate when mixed in solution. It is known that chitosan is non-toxic and has antimicrobial properties and so these results can be compared against the lysozyme and Nafion tests. The overall adhesion of material for 3 bilayers of Nafion/chitosan (pH=5) was higher than other results as the frequency changed by around 2400Hz. In addition to this a LbL assembly consisting of lysozyme, chitosan and Nafion was constructed. Similarly to the Nafion and chitosan test, there was lower repeatability in the results as there was no obvious trends.

Contact angle measurements were taken to test the hydrophobicity of each of the LbL systems created. The 3 bilayers of Nafion/chitosan (pH=5) coating showed the highest contact angle of 60.76° . From the AFM results it can be said that the coatings have a significant number of peaks and troughs in the topography which could be the reason for the low hydrophobicity.

It was observed that 6 bilayers of Nafion/lysozyme (pH 6.2) exhibited the greatest antimicrobial resistance against *S. aureus* and *E. coli*, inhibiting their growth by 100%. Significant antimicrobial activity was also observed for the systems comprising 3 bilayers of Nafion/chitosan (pH=5) and the lysozyme, chitosan Nafion tri-component.

A final experiment was done to test how visible each test was in a transparency test. Nafion/lysozyme tests that used more neutral pH's absorbed more light which indicated they were more visible. The Nafion/chitosan system had the lowest absorbance. The lysozyme, chitosan and Nafion tri-component assembly had the second lowest absorbance.

5. Conclusion

In conclusion, this study provides direct evidence that LbL assemblies based on Nafion can open a very promising avenue in the field of antimicrobial coatings, giving rise to a range of nanostructured materials that are stable, reliable and non-toxic.

Further work would involve a more systematic approach including more combinations of pH's, number of layers and materials. An aim would be to create larger contact angles and make the surface coatings less visible whilst retaining the high antimicrobial effect.

References

- [1] Wise, R., Hart, T., Cars, O., Streulens, Marc., Helmuth, R., and Huovinen, P. (1998). Antimicrobial resistance is a major threat to public health. *British Medical Journal*. 1 (1), pp609.
- [2] de Villiers, M., Otto, D., Strydom, S. and Lvov, Y. (2011). Introduction to nanocoatings produced by layer-by-layer (LbL) self-assembly. *Advanced Drug Delivery Reviews*, 63(9), pp.701-715.
- [3] Karan, C. (2016). What are Anti Fouling Paints and TBT?. [online] Available at: <http://www.marineinsight.com/environment/what-are-anti-fouling-paints-and-tbt> [Accessed 20 Dec. 2016].
- [4] Page, K., Wilson, M. and Parkin, I. (2009). Antimicrobial surfaces and their potential in reducing the role of the inanimate environment in the incidence of hospital-acquired infections. *Journal of Materials Chemistry*, 19(23), pp.3819.
- [5] Villanueva, M., González, J., Rodríguez-Castellón, E., Teves, S and Copello, G. (2016). Antimicrobial surface functionalization of PVC by a guanidine based antimicrobial polymer. *Materials Science and Engineering: C*. 67 (1), pp.214–220.
- [6] Harrison, J., Turner, R., Joo, D., Stan, M., Chan, C., Allan, N., Vrionis, H., Olson, M. and Ceri, H. (2008). Copper and Quaternary Ammonium Cations Exert Synergistic Bactericidal and Antibiofilm Activity against *Pseudomonas aeruginosa*. *Antimicrobial Agents and Chemotherapy*, 52(8), pp.2870-2881.
- [7] Grass, G., Rensing, C. and Solioz, M. (2010). Metallic Copper as an Antimicrobial Surface. *Applied and Environmental Microbiology*, 77(5), pp.1541-1547.
- [8] Wrona, A., Bilewska, K., Lis, M., Kamińska, M., Olszewski, T., Pajzderski, P., Więclaw, G., Jaśkiewicz, M. and Kamysz, W. (2017). Antimicrobial properties of protective coatings produced by plasma spraying technique. *Surface and Coatings Technology*, 318, pp.332-340.
- [9] Lewis, A and Keevil, C. (2004). Antibacterial properties of alloys and its alloys in HVAC&R systems. *International Cooper Association* 1 (1), pp.4-41.

- [10] Yoshida, Y., Furuta, S. and Niki, E. (1993). Effects of metal chelating agents on the oxidation of lipids induced by copper and iron. *Biochimica et Biophysica Acta (BBA) - Lipids and Lipid Metabolism*, 1210(1), pp.81-88
- [11] Mu, Q., Jiang, G., Chen, L., Zhou, H., Fourches, D., Tropsha, A. and Yan, B. (2014). Chemical Basis of Interactions Between Engineered Nanoparticles and Biological Systems. *Chemical Reviews*, 114(15), pp.7740-7781.
- [12] Trinchi, A., Yang, Y., Tulloh, A., Zahiri, S. and Jahedi, M. (2011). Copper Surface Coatings Formed by the Cold Spray Process: Simulations Based on Empirical and Phenomenological Data. *Journal of Thermal Spray Technology*, 20(5), pp.986-991.
- [13] Champagne, V and Helfritsch, D (2013). A demonstration of the antimicrobial effectiveness of various copper surfaces. *J. Biol. Eng.*, 7 (1), p. 8.
- [14] Sharifahmadian, O., Salimijazi, H., Fathi, M., Mostaghimi, J. and Pershin, L. (2012). Study of the Antibacterial Behavior of Wire Arc Sprayed Copper Coatings. *Journal of Thermal Spray Technology*, 22(2-3), pp.371-379.
- [15] Sharifahmadian, O., Salimijazi, H., Fathi, M., Mostaghimi, J and Pershin, L (2013) Relationship between surface properties and antibacterial behaviour of wire arc spray copper coatings. *Surf. Coat. Technol.*, 233. p. 74–79.
- [16] Salgado, C., Sepkowitz, K., John, J., Cantey, J., Attaway, H., Freeman, K., Sharpe, P., Michels, H. and Schmidt, M. (2013). Copper Surfaces Reduce the Rate of Healthcare-Acquired Infections in the Intensive Care Unit. *Infection Control & Hospital Epidemiology*, 34(05), pp.479-486.
- [17] Kim, J., Kuk, E., Yu, K., Kim, J., Park, S., Lee, H., Kim, S., Park, Y., Park, Y., Hwang, C., Kim, Y., Lee, Y., Jeong, D and Cho, M (2007). Antimicrobial effects of silver nanoparticles. *Nanomedicine: Nanotechnology, Biology and Medicine*. 3 (1), p95–101.
- [18] Chen, Y., Hsu, C & He, J (2013). Antibacterial silver coating on poly(ethylene terephthalate) fabric by using high power impulse magnetron sputtering. *Surface and Coatings Technology*. 232 (1), p868–875.

- [19] McGillicuddy, E., Murray, I., Kavanagh, S., Morrison, L., Fogarty, A., Cormican, M., Dockery, P., Prendergast, M., Rowan, N & Morris, D (2016). Science of The Total Environment. *Silver nanoparticles in the environment: Sources, detection and ecotoxicology*. 575 (1), p1.
- [20] Barrett, S. (2005). *Colloidal Silver: Risk Without Benefit*. Available: <http://www.quackwatch.org/01QuackeryRelatedTopics/PhonyAds/silverad.html>. Last accessed 15/12/2016.
- [21] Cooper, J. (1988). Review of the environmental toxicity of quaternary ammonium halides. *Ecotoxicology and Environmental Safety*, 16(1), pp.65-71.
- [22] Liu, S., Tonggu, L., Niu, L., Gong, S., Fan, B., Wang, L., Zhao, J., Huang, C., Pashley, D. and Tay, F. (2016). Antimicrobial activity of a quaternary ammonium methacryloxy silicate-containing acrylic resin: a randomised clinical trial. *Scientific Reports*, 6(1).
- [23] Zhanga, A., Liu, Q., Lei, Y., Hong, S and Lin, Y. (2015). Synthesis and antimicrobial activities of acrylamide polymers containing quaternary ammonium salts on bacteria and phytopathogenic fungi. *Reactive and Functional Polymers*. 88 (1), p39–46.
- [24] Carmona-Ribeiro, A. and de Melo Carrasco, L. (2013). Cationic Antimicrobial Polymers and Their Assemblies. *International Journal of Molecular Sciences*, 14(5), pp.9906-9946.
- [25] Lundin, J., Coneska, P., Fulmer, P & Wynne, J. (2014). Relationship between surface concentration of amphiphilic quaternary ammonium biocides in electrospun polymer fibres and biocidal activity. *Reactive and Functional Polymers*. 77 (1), p39-46.
- [26] Tor, Y. and Fair, R. (2014). Antibiotics and Bacterial Resistance in the 21st Century. *Perspectives in Medicinal Chemistry*, p.25.
- [27] Lvov, Y., Ariga, K., Onda, M., Ichinose, I. and Kunitake, T. (1999). A careful examination of the adsorption step in the alternate layer-by-layer assembly of linear polyanion and polycation. *Colloids and Surfaces A: Physicochemical and Engineering Aspects*, 146(1-3), pp.337-346.

- [28] Decher, G. (1997). Fuzzy Nanoassemblies: Toward Layered Polymeric Multicomposites. *Science*, 277(5330), pp.1232-1237.
- [29] Xiang, Y., Lu, S. and Jiang, S. (2012). Layer-by-layer self-assembly in the development of electrochemical energy conversion and storage devices from fuel cells to supercapacitors. *Chemical Society Reviews*, 41(21), p.7291.
- [30] Chen, D., Zhang, Y., Bessho, T., Sang, J., Hirahara, H., Mori, K. and Kang, Z. (2016). Layer by layer electroless deposition: An efficient route for preparing adhesion-enhanced metallic coatings on plastic surfaces. *Chemical Engineering Journal*, 303, pp.100-108.
- [31] Linford, M., Auch, M. and Möhwald, H. (1998). Nonmonotonic Effect of Ionic Strength on Surface Dye Extraction during Dye–Polyelectrolyte Multilayer Formation. *Journal of the American Chemical Society*, 120(1), pp.178-182.
- [32] Bertrand, P., Jonas, A., Laschewsky, A. and Legras, R. (2000). Ultrathin polymer coatings by complexation of polyelectrolytes at interfaces: suitable materials, structure and properties. *Macromolecular Rapid Communications*, 21(7), pp.319-348.
- [33] Mundra, P., Otto, T., Gaponik, N. and Eychmüller, A. (2013). Automated setup for spray assisted layer-by-layer deposition. *Review of Scientific Instruments*, 84(7), p.07410
- [34] Bottino, M., Kamocki, K., Yassen, G., Platt, J., Vail, M., Ehrlich, Y., Spolnik, K. and Gregory, R. (2013). Bioactive Nanofibrous Scaffolds for Regenerative Endodontics. *Journal of Dental Research*, 92(11), pp.963-969.
- [35] Nolte, A., Chung, J., Walker, M. and Stafford, C. (2009). In situ Adhesion Measurements Utilizing Layer-by-Layer Functionalized Surfaces. *ACS Applied Materials & Interfaces*, 1(2), pp.373-380.
- [36] Elbert, D., Herbert, C. and Hubbell, J. (1999). Thin Polymer Layers Formed by Polyelectrolyte Multilayer Techniques on Biological Surfaces. *Langmuir*, 15(16), pp.5355-5362.

- [37] Dubas, S. and Schlenoff, J. (1999). Factors Controlling the Growth of Polyelectrolyte Multilayers. *Macromolecules*, 32(24), pp.8153-8160.
- [38] Rmaile, H. and Schlenoff, J. (2002). "Internal pKa's" in Polyelectrolyte Multilayers: Coupling Protons and Salt. *Langmuir*, 18(22), pp.8263-8265.
- [39] Buron, C., Filiâtre, C., Membrey, F., Bainier, C., Buisson, L., Charrat, D. and Foissy, A. (2009). Surface morphology and thickness of a multilayer film composed of strong and weak polyelectrolytes: Effect of the number of adsorbed layers, concentration and type of salts. *Thin Solid Films*, 517(8), pp.2611-2617.
- [40] Schoeler, B., Kumaraswamy, G. and Caruso, F. (2002). Investigation of the Influence of Polyelectrolyte Charge Density on the Growth of Multilayer Thin Films Prepared by the Layer-by-Layer Technique. *Macromolecules*, 35(3), pp.889-897.
- [41] Bieker, P. and Schönhoff, M. (2010). Linear and Exponential Growth Regimes of Multilayers of Weak Polyelectrolytes in Dependence on pH. *Macromolecules*, 43(11), pp.5052-5059.
- [42] Arys, X., Jonas, A., Laguitton, B., Legras, R., Laschewsky, A. and Wischerhoff, E. (1998). Structural studies on thin organic coatings built by repeated adsorption of polyelectrolytes. *Progress in Organic Coatings*, 34(1-4), pp.108-118.
- [43] Kamineni, V., Lvov, Y. and Dobbins, T. (2007). Layer-by-Layer Nanoassembly of Polyelectrolytes Using Formamide as the Working Medium. *Langmuir*, 23(14), pp.7423-7427.
- [44] Ferreira, M. and Rubner, M. (1995). Molecular-Level Processing of Conjugated Polymers. 1. Layer-by-Layer Manipulation of Conjugated Polyions. *Macromolecules*, 28(21), pp.7107-7114.
- [45] Motschmann, H., Stamm, M. and Toprakcioglu, C. (1991). Adsorption kinetics of block copolymers from a good solvent: a two-stage process. *Macromolecules*, 24(12), pp.3681-3688.

- [46] Lei, X., Huang, J., Jin, X., Chen, S. and Zhao, X. (2016). Application of Johnson-Mehl-Avrami-Kolmogorov type equation in non-isothermal phase process: Re-discussion. *Materials Letters*, 181, pp.240-243.
- [47] Romanò, C., Scarponi, S., Gallazzi, E., Romanò, D. and Drago, L. (2015). Antibacterial coating of implants in orthopaedics and trauma: a classification proposal in an evolving panorama. *Journal of Orthopaedic Surgery and Research*, 10(1).
- [48] Shenoy, D. and Sukhorukov, G. (2004). Engineered microcrystals for direct surface modification with layer-by-layer technique for optimized dissolution. *European Journal of Pharmaceutics and Biopharmaceutics*, 58(3), pp.521-527.
- [49] Song, W., He, Q., Möhwald, H., Yang, Y. and Li, J. (2009). Smart polyelectrolyte microcapsules as carriers for water-soluble small molecular drug. *Journal of Controlled Release*, 139(2), pp.160-166.
- [50] Schüler, C. and Caruso, F. (2001). Decomposable Hollow Biopolymer-Based Capsules. *Biomacromolecules*, 2(3), pp.921-926.
- [51] Dubas, S., Farhat, T. and Schlenoff, J. (2001). Multiple Membranes from "True" Polyelectrolyte Multilayers. *Journal of the American Chemical Society*, 123(22), pp.5368-5369.
- [52] Sukhishvili, S. and Granick, S. (2000). Layered, Erasable, Ultrathin Polymer Films. *Journal of the American Chemical Society*, 122(39), pp.9550-9551
- [53] Cho, J. and Caruso, F. (2003). Polymeric Multilayer Films Comprising Deconstructible Hydrogen-Bonded Stacks Confined between Electrostatically Assembled Layers. *Macromolecules*, 36(8), pp.2845-2851.
- [54] Kim, Y., Collins, R., Wedam, K and Allara, D (1991). Real Time Spectroscopic Ellipsometry: In Situ Characterization of Pyrrole Electropolymerization. *Journal of The Electrochemical Society*, 138(11), p.3266.
- [55] Vázquez, E., Dewitt, D., Hammond, P. and Lynn, D. (2002). Construction of Hydrolytically-Degradable Thin Films via Layer-by-Layer Deposition of Degradable Polyelectrolytes. *Journal of the American Chemical Society*, 124(47), pp.13992-13993.

- [56] Tullberg, M (2015). *Patent US20150024157 - Fouling release coatings*. [online] Available at: <https://www.google.com/patents/US20150024157> [Last accessed 14/12/2016.]
- [57] Chambers, L., Stokes, K., Walsh, F. and Wood, R. (2007). Corrigendum to “Modern approaches to marine antifouling coatings” [Surf. Coat. Technol. 201 (2006) 3642–3652]. *Surface and Coatings Technology*, 202(2), pp.412-413.
- [58] Liu, X. and Picart, C. (2015). Layer-by-Layer Assemblies for Cancer Treatment and Diagnosis. *Advanced Materials*, 28(6), pp.1295-1301.
- [59] [Poverenov, E., Rutenberg, R., Danino, S., Horev, B. and Rodov, V. (2014). Gelatin-Chitosan Composite Films and Edible Coatings to Enhance the Quality of Food Products: Layer-by-Layer vs. Blended Formulations. *Food and Bioprocess Technology*, 7(11), pp.3319-3327.
- [60] Bovey, F. (2012). *Macromolecules*. Burlington: Elsevier Science. p486
- [61] Coradin, T., Coupé, A. and Livage, J. (2003). Interactions of bovine serum albumin and lysozyme with sodium silicate solutions. *Colloids and Surfaces B: Biointerfaces*, 29(2-3), pp.189-196
- [62] The Protein Data Bank H.M. Berman, J. Westbrook, Z. Feng, G. Gilliland, T.N. Bhat, H. Weissig, I.N. Shindyalov, P.E. Bourne (2000) *Nucleic Acids Research*, 28: 235-242
- [63] Bovey, F. (2012). *Macromolecules*. Burlington: Elsevier Science. p123
- [64] Blake, C., Koenig, D., Mair, G., North, A., Phillips, D. and Sarma, V. (1965). Structure of Hen Egg-White Lysozyme: A Three-dimensional Fourier Synthesis at 2 Å Resolution. *Nature*, 206(4986), pp.757-761.
- [65] Kubiak-Ossowska, K. and Mulheran, P. (2010). Mechanism of Hen Egg White Lysozyme Adsorption on a Charged Solid Surface. *Langmuir*, 26(20), pp.15954-15965.
- [66] Xu, K., Ouberai, M. and Welland, M. (2013). A comprehensive study of lysozyme adsorption using dual polarization interferometry and quartz crystal microbalance with dissipation. *Biomaterials*, 34(5), pp.1461-1470.

- [67] Daly, S., Przybycien, T. and Tilton, R. (2003). Coverage-Dependent Orientation of Lysozyme Adsorbed on Silica. *Langmuir*, 19(9), pp.3848-3857.
- [68] Phillips, D. (1966). The Three-Dimensional Structure of an Enzyme Molecule. *Scientific American*, 215(5), pp.78-90.
- [69] Ramachandran, G. and Venkatachalam, C. (1968). Stereochemical criteria for polypeptides and proteins. IV. Standard dimensions for the cis-peptide unit and conformation of cis-polypeptides. *Biopolymers*, 6(9), pp.1255-1262.
- [70] Sears, D. (2017). Hen Egg White Lysozyme: Overview of Function and Structure. [online] Biosci.mcdb.ucsb.edu. Available at: <https://biosci.mcdb.ucsb.edu/biochemistry/tw-enz/lysozyme/HEWL/lysozyme-overview.htm> [Accessed 10 Aug. 2017].
- [71] Phillips, D. (1966). The Three-Dimensional Structure of an Enzyme Molecule. *Scientific American*, 215(5), pp.78-90.
- [72] Vocadlo, D., Davies, G., Laine, R. and Withers, S. (2001). Catalysis by hen egg-white lysozyme proceeds via a covalent intermediate. *Nature*, 412(6849), pp.835-838.
- [73] Held, J. and van Smaalen, S. (2014). The active site of hen egg-white lysozyme: flexibility and chemical bonding. *Acta Crystallographica Section D Biological Crystallography*, 70(4), pp.1136-1146.
- [74] Phizicky, E. and Fields, S. (1995) Protein–protein interactions: methods for detection and analysis, *Microbiological Reviews*, 59, pp. 94-123.
- [75] Koshland, D. (1953). Stereochemistry and The Mechanism Of Enzymatic Reactions. *Biological Reviews*, 28(4), pp.416-436.
- [76] Davies, G. and Henrissat, B. (1995). Structures and mechanisms of glycosyl hydrolases. *Structure*, 3(9), pp.853-859.
- [77] Permapure.com. (2017). Nafion: Physical and Chemical Properties – Perma Pure LLC. [online] Available at: <http://www.permapure.com/products/nafion-tubing/nafion-physical-and-chemical-properties/> [Accessed 15 Aug. 2017].

- [78] Zhong, L., Pang, L., Che, L., Wu, X. and Chen, X. (2013). Nafion coated stainless steel for anti-biofilm application. *Colloids and Surfaces B: Biointerfaces*, 111, pp.252-256.
- [79] Rodgers, M., Bonville, L., Kunz, H., Slattery, D. and Fenton, J. (2012). Fuel Cell Perfluorinated Sulfonic Acid Membrane Degradation Correlating Accelerated Stress Testing and Lifetime. *Chemical Reviews*, 112(11), pp.6075-6103.
- [80] O'Rourke, C., Klyuzhin, I., Park, J. and Pollack, G. (2011). Unexpected water flow through Nafion-tube punctures. *Physical Review E*, 83(5).
- [81] Zhang, H., Pan, J., He, X. and Pan, M. (2007). Zeta potential of Nafion molecules in isopropanol-water mixture solvent. *Journal of Applied Polymer Science*, 107(5), pp.3306-3309.
- [82] Heitner-Wirguin, C. (1996). Recent advances in perfluorinated ionomer membranes: structure, properties and applications. *Journal of Membrane Science*, 120(1), pp.1-33
- [83] Kellarakis, A. and Giannelis, E. (2011). Nafion as Cosurfactant: Solubilization of Nafion in Water in the Presence of Pluronic. *Langmuir*, 27(2), pp.554-560.
- [84] Texter, J. (2005). *Reactions and Synthesis in Surfactant Systems*. 1st ed. New York: Taylor & Francis, p.652.
- [85] Chen, Q. and Schmidt-Rohr, K. (2004). ¹⁹F and ¹³C NMR Signal Assignment and Analysis in a Perfluorinated Ionomer (Nafion) by Two-Dimensional Solid-State NMR. *Macromolecules*, 37(16), pp.5995-6003.
- [86] Shao, L. and Titman, J. (2007). CAESURA Studies of Helical Jump Motions in Semi-Crystalline Polymers. *Macromolecular Chemistry and Physics*, 208(19–20), pp.2055-2065.
- [87] Schmidt-Rohr, K. and Chen, Q. (2007). Parallel cylindrical water nanochannels in Nafion fuel-cell membranes. *Nature Materials*, 7(1), pp.75-83.
- [88] Ho, M. (2012). Super-Conducting Liquid Crystalline Water Aligned with Collagen Fibres in the Fascia as Acupuncture Meridians of Traditional Chinese Medicine. *Forum on Immunopathological Diseases and Therapeutics*, 3(3-4), pp.221-236.

- [89] Li Q., Dunn E.T., Grandmaison E.W., Goosen M. (1992). Applications and Properties of Chitosan, *J. Journal of Bioactive and Compatible Polymers*. 71, pp.370–39.
- [90] Sagheer, F., Al-Sughayer, M., Muslim, S. and Elsabee, M. (2009). Extraction and characterization of chitin and chitosan from marine sources in Arabian Gulf. *Carbohydrate Polymers*, 77(2), pp.410-419.
- [91] Klaykruayat, B., Siralertmukul, K. and Srikulkit, K. (2010). Chemical modification of chitosan with cationic hyperbranched dendritic polyamidoamine and its antimicrobial activity on cotton fabric. *Carbohydrate Polymers*, 80(1), pp.197-207.
- [92] Lim, S. and Hudson, S. (2004). Synthesis and antimicrobial activity of a water-soluble chitosan derivative with a fiber-reactive group. *Carbohydrate Research*, 339(2), pp.313-319.
- [93] Rahman Bhuiyan, M., Hossain, M., Zakaria, M., Islam, M. and Zulhash Uddin, M. (2016). Chitosan Coated Cotton Fiber: Physical and Antimicrobial Properties for Apparel Use. *Journal of Polymers and the Environment*, 25(2), pp.334-342.
- [94] Kubota, N. and Eguchi, Y. (1997). Facile Preparation of Water-Soluble N-Acetylated Chitosan and Molecular Weight Dependence of Its Water-Solubility. *Polymer Journal*, 29(2), pp.123-127.
- [95] Rinaudo, M., Pavlov, G. and Desbrières, J. (1999). Influence of acetic acid concentration on the solubilization of chitosan. *Polymer*, 40(25), pp.7029-7032.
- [96] Rinaudo, M., Pavlov, G. and Desbrières, J. (1999). Solubilization of Chitosan in Strong Acid Medium. *International Journal of Polymer Analysis and Characterization*, 5(3), pp.267-276.
- [97] Senthilkumar, S., Rajesh, S., Jayalakshmi, A., Aishwarya, G. and Raju Mohan, D. (2012). Preparation and performance evaluation of poly (ether-imide) incorporated polysulfone hemodialysis membranes. *Journal of Polymer Research*, 19(6).
- [98] Evans, E. and Kent, S. (1962). The use of basic polysaccharides in histochemistry and cytochemistry: iv. Precipitation and agglutination of biological materials by

aspergillus polysaccharide and deacetylated chitin. *Journal of histochemistry & cytochemistry*, 10(1), pp.24-28.

[99] Rahman Bhuiyan, M., Hossain, M., Zakaria, M., Islam, M. and Zulhash Uddin, M. (2016). Chitosan Coated Cotton Fiber: Physical and Antimicrobial Properties for Apparel Use. *Journal of Polymers and the Environment*, 25(2), pp.334-342.

[100] Dutta, P., Tripathi, S., Mehrotra, G. and Dutta, J. (2009). Perspectives for chitosan based antimicrobial films in food applications. *Food Chemistry*, 114(4), pp.1173-1182.

[101] Brine, C. (1992). *Advances in chitin and chitosan*. London: Elsevier, p.543.

[102] Rinaudc, M., Pavlov, G. and Desbrières, J. (1999). Solubilization of Chitosan in Strong Acid Medium. *International Journal of Polymer Analysis and Characterization*, 5(3), pp.267-276.

[103] Domard, A. (1987). pH and c.d. measurements on a fully deacetylated chitosan: application to Cull—polymer interactions. *International Journal of Biological Macromolecules*, 9(2), pp.98-104.

[104] Rinaudo, M., Pavlov, G. and Desbrières, J. (1999). Influence of acetic acid concentration on the solubilization of chitosan. *Polymer*, 40(25), pp.7029-7032.

[105] Aiba, S. (1991). Studies on chitosan: 3. Evidence for the presence of random and block copolymer structures in partially N-acetylated chitosans. *International Journal of Biological Macromolecules*, 13(1), pp.40-44.

[106] Kurita, K. (2001). Controlled functionalization of the polysaccharide chitin. *Progress in Polymer Science*, 26(9), pp.1921-1971.

[107] Islam, S., Bhuiyan, M. and Islam, M. (2016). Chitin and Chitosan: Structure, Properties and Applications in Biomedical Engineering. *Journal of Polymers and the Environment*, 25(3), pp.854-866.

[108] Kim, S. and Rajapakse, N. (2005). Enzymatic production and biological activities of chitosan oligosaccharides (COS): A review. *Carbohydrate Polymers*, 62(4), pp.357-368.

- [109] Roberts, G. (1992) Chitin chemistry. Macmillan Press Ltd., London
- [110] Mima, S., Miya, M., Iwamoto, R. and Yoshikawa, S. (1983). Highly deacetylated chitosan and its properties. *Journal of Applied Polymer Science*, 28(6), pp.1909-1917.
- [111] Kasaai, M. (2009). Various Methods for Determination of the Degree of N-Acetylation of Chitin and Chitosan: A Review. *Journal of Agricultural and Food Chemistry*, 57(5), pp.1667-1676.
- [112] Chenite, A. (2001). Rheological characterisation of thermogelling chitosan/glycerol-phosphate solutions. *Carbohydrate Polymers*, 46(1), pp.39-47.
- [113] Saïed, N. and Aider, M. (2014). Zeta Potential and Turbidimetry Analyzes for the Evaluation of Chitosan/Phytic Acid Complex Formation. *Journal of Food Research*, 3(2), p.71.
- [114] Lee, S., Lim, S., Lim, E. and Lee, K. (2010). Synthesis of aqueous dispersion of graphenes via reduction of graphite oxide in the solution of conductive polymer. *Journal of Physics and Chemistry of Solids*, 71(4), pp.483-486.
- [115] Dawson, R., Elliot, D., Elliot, W. and Jones, K. (1986). *Data for Biochemical Research*. Oxford Science Publications. 3(1).
- [116] Rubenhag, C. (2016). *Q-Sense*. Available: <http://www.biolinscientific.com/q-sense/>. Last accessed 05/12/2016.
- [117] Dixon, M. (2008). Quartz Crystal Microbalance with Dissipation Monitoring: Enabling Real-Time Characterization of Biological Materials and their Interactions. *Journal of biomolecular techniques*. 19 (3), pp151-158.
- [118] Sauerbrey G. (1959). The use of quartz crystal oscillators for weighing thin layers and for microweighing. *Z. Phys.* 155. pp206–222
- [119] Keller, C and Kasemo, B. (1998). Surface Specific Kinetics of Lipid Vesicle Adsorption Measured with a Quartz Crystal Microbalance. *Biophysical Journal*, 75(3), pp.1397-1402.
- [120] Ossila. (2017). Spin Coating: A Guide to Theory and Techniques. [online] Available at: <https://www.ossila.com/pages/spin-coating> [Accessed 21 Aug. 2017].

- [121] Sahu, N., Parija, B. and Panigrahi, S. (2009). Fundamental understanding and modeling of spin coating process: A review. *Indian Journal of Physics*, 83(4), pp.493-502.
- [122] Marx, K. (2003). Quartz Crystal Microbalance: A Useful Tool for Studying Thin Polymer Films and Complex Biomolecular Systems at the Solution–Surface Interface. *Biomacromolecules*, 4(5), pp.1099-1120.
- [123] Salam, A., Makhoulouf, H and Tiginyanu, I (2011). *Nanocoatings and ultra thin films*. Oxford: Woodhead Publishing. (1) p141.
- [124] Poon, C. and Bhushan, B. (1995). Comparison of surface roughness measurements by stylus profiler, AFM and non-contact optical profiler. *Wear*, 190(1), pp.76-88.
- [125] Rivero, S., A. Garcia, M. and Pinotti, A. (2014). Microstructural Characterization Of Chitosan Films Used As Support For Ferulic Acid Release. *Advanced Materials Letters*, 5(10), pp.578-586.
- [126] Yuan, Y. and Lee, T. (2013) Contact Angle and Wetting Properties. In: Bracco, G. and Holst, B., Eds., *Surface Science Techniques Springer Series, Surface Sciences*. Springer Berlin Heidelberg. mBerlin and Heidelberg, (51) pp3-34.
- [127] Bradley, M. (2016). *FTIR Sample Techniques - Transmission*. Available: <https://www.thermofisher.com/uk/en/home/industrial/spectroscopy-elemental-isotope-analysis/spectroscopy-elemental-isotope-analysis-learning-center/molecular-spectroscopy-information/ftir-information/f>. Last accessed 07/12/2016
- [128] Hiller, M. (2016). *FTIR Analysis*. Available: <https://www.labtesting.com/services/polymer-testing/ftir-analysis/>. Last accessed 07/12/2016

- [129] Choudhary, O. and ka, P. (2017). Scanning Electron Microscope: Advantages and Disadvantages in Imaging Components. *International Journal of Current Microbiology and Applied Sciences*, 6(5), pp.1877-1882.
- [130] Tissue, B. (2012). Ultraviolet and Visible Absorption Spectroscopy. *Characterization of Materials*. (1)1. pp1–13.
- [131] Lu, Z., Rong, K., Li, J., Yang, H. and Chen, R. (2013). Size-dependent antibacterial activities of silver nanoparticles against oral anaerobic pathogenic bacteria. *Journal of Materials Science: Materials in Medicine*, 24(6), pp.1465-1471.
- [132] Amara, C., Eghbal, N., Degraeve, P. and Gharsallaoui, A. (2016). Using complex coacervation for lysozyme encapsulation by spray-drying. *Journal of Food Engineering*, 183, pp.50-57.
- [133] Lin, S., Chang, C., Chang, J. and Mammel, K. (2014). Comparison of Dye Adsorption of Three Forms of Chitosan. *Advances in Chemical Engineering and Science*, 04(03), pp.319-326.
- [134] Fernandes, L., Resende, C., Tavares, D., Soares, G., Castro, L. and Granjeiro, J. (2011). Cytocompatibility of chitosan and collagen-chitosan scaffolds for tissue engineering. *Polímeros*, 21(1), pp.1-6
- [135] Höök, F., Kasemo, B., Nylander, T., Fant, C., Sott, K. and Elwing, H. (2001). Variations in Coupled Water, Viscoelastic Properties, and Film Thickness of a Mefp-1 Protein Film during Adsorption and Cross-Linking: A Quartz Crystal Microbalance with Dissipation Monitoring, Ellipsometry, and Surface Plasmon Resonance Study. *Analytical Chemistry*, 73(24), pp.5796-5804.
- [136] Fernandes, D., Kluska, W., Stanislawski, J., Board, B., Krysmann, M. and Kellarakis, A. (2017). Novel hydrogels containing Nafion and poly(ethylene oxide) based block copolymers. *Polymer*, 114, pp.73-78.
- [137] Gleason, W. (2013). *Fuel cell technician's guide*. Clifton Park, NY: Delmar, p.94.

- [138] Dolinsky, T., Nielsen, J., McCammon, J. and Baker, N. (2004). PDB2PQR: an automated pipeline for the setup of Poisson-Boltzmann electrostatics calculations. *Nucleic Acids Research*, 32(Web Server), pp.W665-W667
- [139] Yu, G., Liu, J. and Zhou, J. (2015). Mesoscopic coarse-grained simulations of hydrophobic charge induction chromatography (HCIC) for protein purification. *AIChE Journal*, 61(6), pp.2035-2047.
- [140] Nezu, T., Masuyama, T., Sasaki, K., Saitoh, S., Taira, M. and Araki, Y. (2008). Effect of pH and Addition of Salt on the Adsorption Behavior of Lysozyme on Gold, Silica, and Titania Surfaces Observed by Quartz Crystal Microbalance with Dissipation Monitoring. *Dental Materials Journal*, 27(4), pp.573-580.
- [141] Davies, R., Neuberger, A. and Wilson, B. (1969). The dependence of lysozyme activity on pH and ionic strength. *Biochimica et Biophysica Acta (BBA) - Enzymology*, 178(2), pp.294-305
- [142] R. R. L. De Oliveira, D. A. C. Albuquerque, F. L. Leite, F. M. Yamaji and T. G. S. Cruz (2012). *Measurement of the Nanoscale Roughness by Atomic Force Microscopy: Basic Principles and Applications*. 1st ed. INTECH Open Access Publisher, pp.148-173.
- [143] Haggerty, L. and Lenhoff, A. (1993). Analysis of ordered arrays of adsorbed lysozyme by scanning tunneling microscopy. *Biophysical Journal*, 64(3), pp.886-895
- [144] Ramsden, J., Bachmanova, G. and Archakov, A. (1994). Kinetic evidence for protein clustering at a surface. *Physical Review E*, 50(6), pp.5072-5076.
- [145] Nygren, H., Alaeddin, S., Lundström, I. and Magnusson, K. (1994). Effect of surface wettability on protein adsorption and lateral diffusion. Analysis of data and a statistical model. *Biophysical Chemistry*, 49(3), pp.263-272
- [146] Kim, D., Blanch, H. and Radke, C. (2002). Direct Imaging of Lysozyme Adsorption onto Mica by Atomic Force Microscopy. *Langmuir*, 18(15), pp.5841-5850
- [147] Pace, S., Vasani, R., Zhao, W., Perrier, S. and Voelcker, N. (2014). Photonic porous silicon as a pH sensor. *Nanoscale Research Letters*, 9(1), p.420.

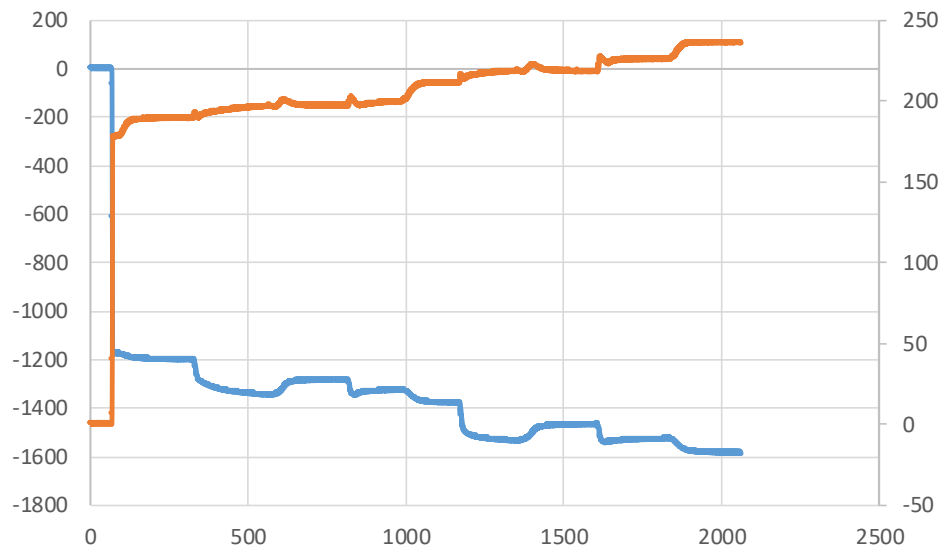
- [148] Abe, Y., Ueda, T., Iwashita, H., Hashimoto, Y., Motoshima, H., Tanaka, Y. and Imoto, T. (1995). Effect of Salt Concentration on the pKa of Acidic Residues in Lysozyme. *Journal of Biochemistry*, 118(5), pp.946-952.
- [149] Kim, M., Park, S., Gu, B. and Kim, C. (2015). Fabrication of Chitosan Nanofibers Scaffolds with Small Amount Gelatin for Enhanced Cell Viability. *Applied Mechanics and Materials*, 749, pp.220-224.
- [150] Wenzel, R. (1936). Resistance of solid surfaces to wetting by water. *Industrial & Engineering Chemistry*, 28(8), pp.988-994.
- [151] Lu, Z., Dockery, C., Crosby, M., Chavarria, K., Patterson, B. and Giedd, M. (2016). Antibacterial Activities of Wasabi against *Escherichia coli* O157:H7 and *Staphylococcus aureus*. *Frontiers in Microbiology*, 7.
- [152] Wecke, J., Lahav, M., Ginsburg, I. and Giesbrecht, P. (1982). Cell wall degradation of *Staphylococcus aureus* by lysozyme. *Archives of Microbiology*, 131(2), pp.116-123.
- [153] Kesel, S., Mader, A., Seeberger, P., Lieleg, O. and Opitz, M. (2014). Carbohydrate Coating Reduces Adhesion of Biofilm-Forming *Bacillus subtilis* to Gold Surfaces. *Applied and Environmental Microbiology*, 80(19), pp.5911-5917.
- [154] Escárega-Galaz, A., López-Cervantes, J., Sánchez-Machado, D., Brito-Zurita, O. and Campas-Baypoli, O. (2017). Antimicrobial Activity of Chitosan Membranes Against *Staphylococcus Aureus* of Clinical Origin. The Rise of Virulence and Antibiotic Resistance in *Staphylococcus aureus*.
- [155] Layne, E. (1957). Spectrophotometric and turbidimetric methods for measuring proteins. *Methods in Enzymology*, pp.447-454
- [156] Stoscheck, C. (1990). Quantitation of protein. *Methods in Enzymology*, pp.50-68
- [157] Deligöz, H., Yilmaztürk, S., Yilmazoğlu, M. and Damyan, H. (2010). The effect of self-assembled multilayer formation via LbL technique on thermomechanical and transport properties of Nafion®112 based composite membranes for PEM fuel cells. *Journal of Membrane Science*, 351(1-2), pp.131-140.

[158] Kumirska, J., Czerwicka, M., Kaczyński, Z., Bychowska, A., Brzozowski, K., Thöming, J. and Stepnowski, P. (2010). Application of Spectroscopic Methods for Structural Analysis of Chitin and Chitosan. *Marine Drugs*, 8(5), pp.1567-1636.

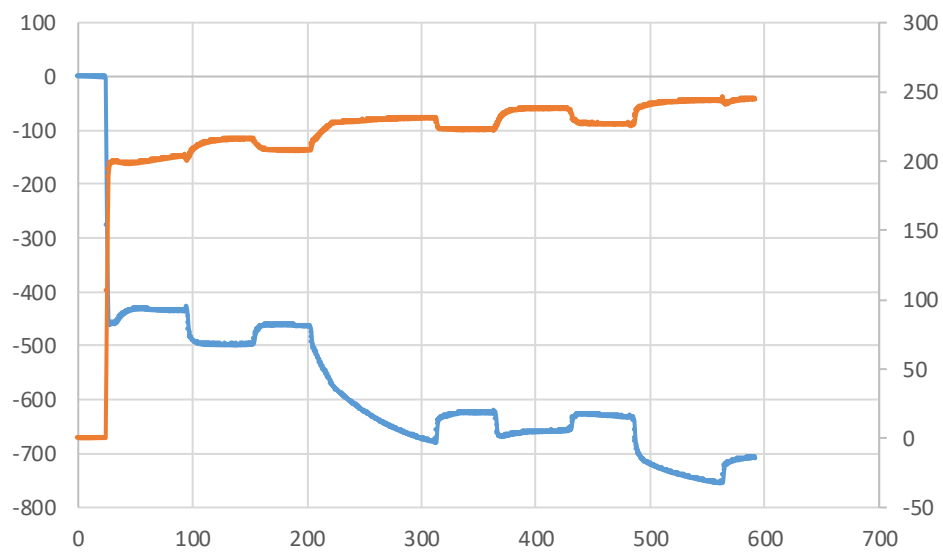
[159] Nagasaka, M., Yoshida, K., Sato, K., Hoshi, T. and Anzai, J. (2010). Electrode potential-dependent colorimetric response of fluorescein-modified layer-by-layer films in the presence of hydrogen peroxide. *Journal of Colloid and Interface Science*, 348(2), pp.441-445

Supplementary Data

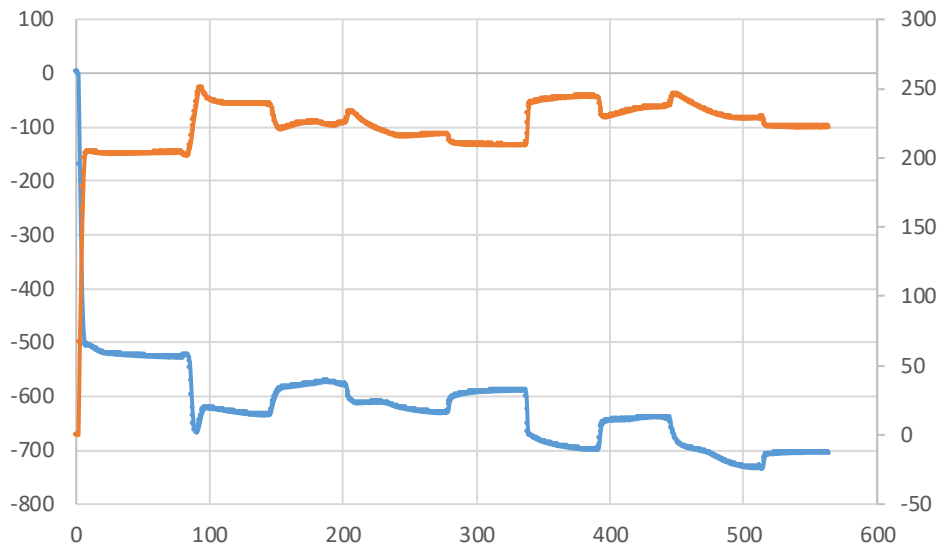
pH 9



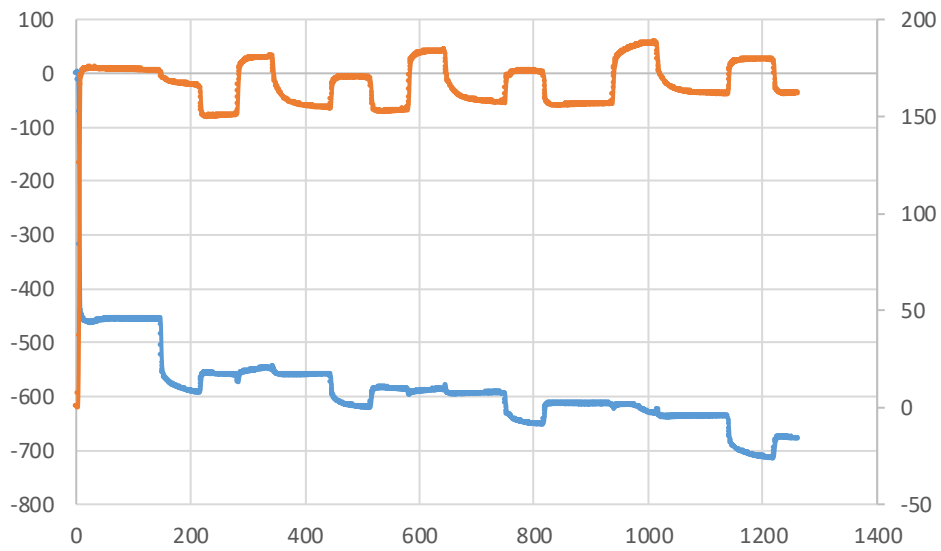
pH 4



pH 7

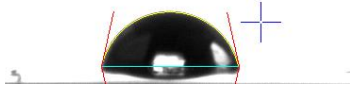


pH 6.2

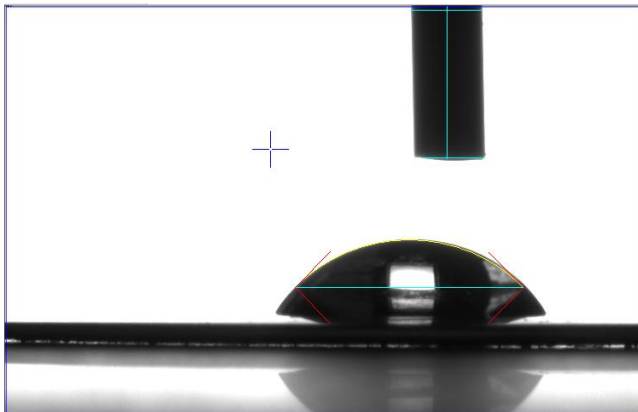


No repeats of Chitosan/Nafion and Lysozyme, Nafion and chitosan attempts.

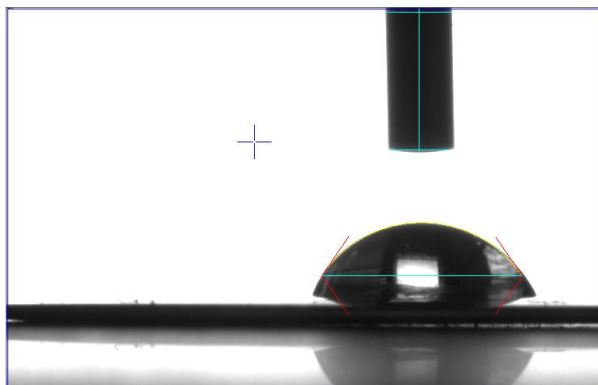
pH 9



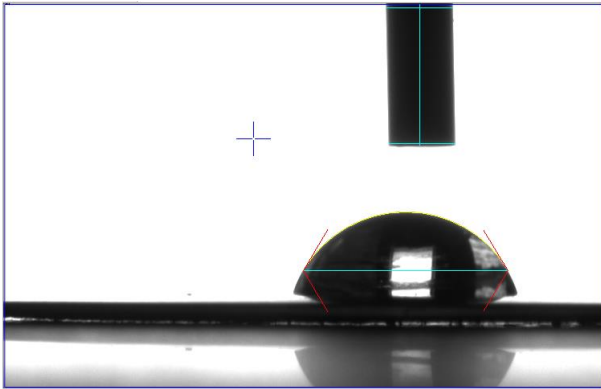
pH 4



pH 6.2



pH 7



Lysozyme, Nafion and Chitosan



Nafion chitosan

